Calvopina Tapia, K., Hinchliffe, P., Brem, J., Heesom, K. J., Johnson, S., Cain, R., ... Avison, M. B. (2017). Structural/mechanistic insights into the efficacy of nonclassical -lactamase inhibitors against extensively drug resistant Stenotrophomonas maltophilia clinical isolates. *Molecular Microbiology*, *106*(3), 492–504. https://doi.org/10.1111/mmi.13831

Structural/mechanistic insights into the efficacy of non-classical β-lactamase inhibitors against extensively drug resistant *Stenotrophomonas maltophilia* clinical isolates.

Karina Calvopiña[1], Philip Hinchliffe[1], Jürgen Brem[2], Kate J. Heesom[3], Samar Johnson[1], Ricky Cain[4], Christopher T. Lohans[2], Colin W. G. Fishwick[4], Christopher J. Schofield[2], James Spencer[1] and Matthew B. Avison[1]*.

[1]School of Cellular & Molecular Medicine, University of Bristol, Bristol, United Kingdom.

[2]Department of Chemistry, University of Oxford, Oxford, United Kingdom.

[3]Bristol University Proteomics Facility, Bristol. United Kingdom.

[4]School of Chemistry, University of Leeds, Leeds. United Kingdom.

***Correspondence to: School of Cellular & Molecular Medicine, University of Bristol, Biomedical Sciences Building, University Walk. Bristol BS81TD, United Kingdom. bimba@bris.ac.uk.**

Running title: β-Lactamase inhibitors versus *S. maltophilia*.

Keywords: antibiotic resistance, proteomics, enzyme inhibition

SUMMARY

Clavulanic acid and avibactam are clinically deployed serine β-lactamase inhibitors, important as a defence against antibacterial resistance. Bicyclic boronates are recently discovered inhibitors of serine and some metallo β-lactamases. Here we show that avibactam and a bicyclic boronate inhibit L2 (serine β-lactamase) but not L1 (metallo β-lactamase) from the extensively drug resistant human pathogen *Stenotrophomonas maltophilia*. X-ray crystallography revealed that both inhibitors bind L2 by covalent attachment to the nucleophilic serine. Both inhibitors reverse ceftazidime resistance in *S. maltophilia* because, unlike clavulanic acid, they do not induce L1 production. Ceftazidime/inhibitor resistant mutants hyper-produce L1, but retain aztreonam/inhibitor susceptibility because aztreonam is not an L1 substrate. Importantly, avibactam, but not the bicyclic boronate is deactivated by L1 at a low rate; the utility of avibactam might be compromised by mutations that increase this deactivation rate. These data rationalize the observed clinical efficacy of ceftazidime/avibactam plus aztreonam as combination therapy for *S. maltophilia* infections and confirm that aztreonam-like β-lactams plus non-classical β-lactamase inhibitors, particularly avibactam-like and bicyclic boronate compounds, have potential for treating infections caused by this most intractable of drug resistant pathogens.

ABBREVIATED SUMMARY

Stenotrophomonas maltophilia **is an important bacterial pathogen that causes severe infections. It can become resistant to all β-lactam antibacterials via mutations that enhance L1 and L2 β-lactamase production. Characterisation of the interactions between various β-lactamase inhibitors and L1 and L2, whole cell susceptibility tests and proteomic analysis of resistant mutants show that the monobactam aztreonam plus the non-β-lactam based β-lactamase inhibitors avibactam and a novel cyclic boronate are excellent combinations against *S. maltophilia.***

INTRODUCTION

β-Lactamases are the most commonly encountered cause of resistance to β-lactams, which are the most frequently prescribed class of antibacterial drug world-wide (Hamad, 2010, Van Boeckel *et al.*, Versporten *et al.*, 2014). β-Lactamases render β-lactams inactive through catalysing efficient hydrolysis of the β-lactam ring (Strynadka *et al.*, 1992, Drawz & Bonomo, 2010). There are many hundreds of known β-lactamases, which are grouped based on sequence and mechanism into the serine β-lactamase (SBL) classes A, C and D, and the metallo-β-lactamase (MBL) subclasses B1, B2 and B3) (Ambler, 1980, Bush, 2013). Broad-spectrum, clinically useful β-lactamase inhibitors are being sought, but the varying chemistries and active site architectures of the different β-lactamase classes makes the development of cross-class inhibitors extremely challenging (King *et al.*, 2016, Brem *et al.*, 2016, Drawz *et al.*, 2014).

Clavulanic acid (**Fig. 1, *top***) is a well-established clinically deployed β-lactam-based inhibitor of, principally, class A SBLs. Clavulanic acid is used in combination with penicillin derivatives such as amoxicillin and ticarcillin, whose bactericidal effects improve against some β-lactamase-carrying isolates of species such as *Escherichia coli* and *Klebsiella pneumoniae* (Al Roomi *et al.*, 1984, Reading & Cole, 1977, Fass & Prior, 1989, Finlay *et al.*, 2003). Clavulanic acid is an irreversible inhibitor of class A enzymes, whose activity arises from fragmentation of the acyl-enzyme complex formed by reaction with the active-site serine nucleophile, to generate a near permanently inactivated species (Sulton *et al.*, 2005). In contrast, avibactam, a recently introduced relatively broad spectrum non-β-lactam-based SBL inhibitor contains a diazobicyclo heterocyclic core structure which reversibly acylates SBLs. The potency of avibactam against class A, C and some class D SBLs is attributed to the stabilization of the carbamoyl complex due to interactions with polar residues present in the active sites, with de-acylation preferentially occurring due to recyclization rather than hydrolytic turnover (Ehmann *et al.*, 2012). This recyclization results in release of intact active

inhibitor rather than an inactive hydrolysis product (**Fig. 1, *middle***) (Stachyra *et al.*, 2010, Coleman, 2011, Wang *et al.*, 2016, Choi *et al.*, 2016). Avibactam has recently been licenced for clinical use in partnership with the oxy-amino cephalosporin ceftazidime, though the combination is not universally efficacious and has no useful activity against MBL-producing bacteria (Coleman, 2011, Abboud *et al.*, 2016).

Boronic acid-based compounds have long been studied as potential SBL inhibitors but, in most cases, are ineffective against MBL targets. For example, the monocyclic boronate vaborbactam (RPX7009) (**Fig. 1, *bottom left***), which has recently been approved for clinical use, is effective against Class A, C and D β-lactamases, but not MBLs (Hecker *et al.*, 2015). However, we recently demonstrated that bicyclic boronate scaffolds can act as potent inhibitors of multiple SBL classes, as well as subclass B1 MBLs (Brem *et al.*, 2016). Accordingly, one method of overcoming the poor activity of ceftazidime/avibactam against MBL producing bacteria would be to combine ceftazidime with a bicyclic boronate inhibitor, such as **2** (**Fig. 1, *bottom right***), or **1**, which is derived from the same scaffold (Cahill *et al.*, 2017). Together, **1** and **2** represent the closest approach to a pan-β-lactamase inhibitor that has, to-date, been reported in the literature (Cahill *et al.*, 2017). Another bicyclic boronate β-lactamase inhibitor (VNRX-5133) has recently completed phase 1 clinical trials (ClinicalTrials.gov, 2016).

Stenotrophomonas maltophilia (Ryan *et al.*, 2009) is one of the most intrinsically multidrug resistant bacterial species encountered in the clinic, causing up to 5% of ventilator associated pneumonias, and around 1% of blood-stream infections. It causes serious infections with high mortality rates in immunocompromised and severely debilitated patients, and colonises the lungs of 20-30% of patients with cystic fibrosis (Brooke, 2012, de Vrankrijker *et al.*, 2010, Looney *et al.*, 2009). While *S. maltophilia* possesses multiple efflux systems (Alonso & Martinez, 2000, Gould & Avison, 2006, Garcia-Leon *et al.*, 2015, Gould *et al.*, 2013) that reduce the net rate of entry for many antimicrobials, β-lactam resistance arises primarily from

production of two β-lactamases, a subclass B3 MBL "L1", which hydrolyses all β-lactams except for the monobactam, aztreonam, and the class A Extended Spectrum SBL (ESBL) "L2", which hydrolyses all first to third generation cephalosporins, all penicillins, and aztreonam (Walsh *et al.*, 1994, Walsh *et al.*, 1997, Gould *et al.*, 2006). The combination of L1 and L2, therefore renders *S. maltophilia* resistant to all β-lactam antibiotics although in clinical practice, ceftazidime can be useful, because most clinical isolates do not produce enough β-lactamase to give resistance (Lemmen *et al.*, 2001, Okazaki & Avison, 2008). Ceftazidime resistant mutants rapidly emerge through hyper-production of L1 and L2, via single site mutations that directly or indirectly activate the L1/L2 transcriptional activator, AmpR (Okazaki & Avison, 2008, Talfan *et al.*, 2013). Accordingly, *S. maltophilia* represents one of the most challenging targets for β-lactam/β-lactamase inhibitor combinations.

Here we report kinetic and structural studies with purified *S. maltophilia* β-lactamases, in vitro testing of various β-lactam/β-lactamase inhibitor combinations against extensively drug resistant clinical *S. maltophilia* isolates, and characterisation of acquired resistance to these combinations. The results reveal that non-classical β-lactamase inhibitors such as avibactam and bicyclic boronates have considerable potential in combatting β-lactam resistance in *S. maltophilia*, particularly when used in combination with aztreonam-like β-lactams.

RESULTS

β-lactamase inhibitors restore aztreonam, but not meropenem activity against S. maltophilia

As a prelude to investigating the effects of β-lactamase inhibitors, we first evaluated the hydrolysis of a range of candidate β-lactams *in vitro* by purified L1 (subclass B3 MBL) and L2 (class A ESBL) under steady state conditions. These data (**Table 1**) reveal the carbapenem meropenem to be predominantly a substrate for L1, with L2 showing only weak hydrolytic

activity, the monobactam aztreonam to be a substrate for L2 only, and that both L1 and L2 can hydrolyse the oxyamino-cephalosporin ceftazidime with similar efficiencies.

We next tested the ability of three β-lactamase inhibitors: clavulanic acid, avibactam and the bicyclic boronate **2** (each at 2 $mg.L^{-1}$) to potentiate the activity of the target β-lactams against *S. maltophilia* (**Table 2**) All three inhibitors reversed aztreonam, but not meropenem resistance in ceftazidime susceptible clinical isolates (K279a, CI-20, CI-29). Furthermore, all three inhibitors reversed ceftazidime and aztreonam, but not meropenem, resistance in a ceftazidime-resistant L1/L2 hyper-producing mutant (K CAZ 10), derived from K279a (**Table 2**) (Talfan *et al.*, 2013)). Interestingly, all three inhibitors were unable to restore ceftazidime susceptibility in a ceftazidime resistant L1/L2 hyper-producing clinical isolate (CI-31), but they all restored aztreonam resistance in CI-31 (**Table 2**).

Efflux pumps play a major role in antimicrobial resistance in *S. maltophilia* (Crossman *et al.*, 2008, Brooke, 2012). Thus, to investigate the possible effect of multi-drug efflux pumps on β-lactamase inhibitor efficacy, we selected two hyper-resistant mutants from the isolate K279a using moxifloxacin and amikacin, known to be efflux pump substrates. Comparative proteomics (**Tables S1, S2, Fig. S1**) confirmed that the two mutants, K MOX 8 and K AMI 32, hyper-produce the SmeDEF and SmeYZ efflux pumps, respectively. In K MOX 8, SmeYZ was downregulated as SmeDEF was hyper-produced, as expected given their reciprocal regulation (Huang *et al.*, 2017). All three β-lactamase inhibitors retained full activity against these efflux pump hyper-producing mutants (**Table 2**) suggesting that efflux does not have a major role in the observed variation in efficacy of the various β-lactam/β-lactamase inhibitor combinations.

The bicyclic boronate 2 does not inhibit the S. maltophilia L1 MBL

Based on these in vitro data we conclude that the bicyclic boronate **2** acts against *S. maltophilia* in a similar fashion to avibactam and clavulanic acid: it reverses aztreonam and, when due to L1/L2 hyper-production, ceftazidime resistance (**Table 2**). As **2** has been shown to inhibit multiple MBLs (Brem *et al.*, 2016), we anticipated that it might also inhibit L1, but the fact that **2** does not reverse resistance to meropenem (**Table 2**), which is predominantly hydrolysed by L1 (**Table 1**) suggests that L1 inhibition by **2** does not occur to a significant extent.

As, to date, the inhibition of subclass B3 MBLs by bicyclic boronates has not been reported, we investigated the inhibition of purified L1 and L2 by the three β-lactamase inhibitors using the fluorogenic β-lactamase substrate FC5 as a new reporter for L1 and L2(van Berkel *et al.*, 2013). Calculated k_{cat}/K_M values clearly demonstrate that FC5 is hydrolysed with a higher efficiency than other β-lactams by both L1 and L2 (**Table 1**). IC_{50} measurements revealed that while all three β-lactamase inhibitors inhibit L2 with nanomolar potencies (**Table 3**), no inhibition of L1 was observed, even when using inhibitor concentrations up to 2.5 mM. NMR spectroscopy confirmed that there is no impact of avibactam or **2** on meropenem hydrolysis by L1 (**Fig S2**). NMR experiments also showed that L1 can hydrolyse avibactam, albeit at a slow rate, but it does not modify **2** to any detectable extent following incubation up to 24 h (**Fig. S3**). Thus, unlike the case for subclass B1 MBLs (Brem *et al.*, 2016), the bicyclic boronate **2** is not an effective inhibitor of the subclass B3 MBL L1.

Structural basis for inhibition of L2 by avibactam and the bicyclic boronate 2

The results above demonstrate that, consistent with the effectiveness of β-lactam/β-lactamase inhibitor combinations against *S. maltophilia* strains, L2 is effectively inhibited by both

avibactam and the bicyclic boronate **2**. To investigate the molecular basis for inhibition of L2 we crystallised the enzyme and soaked the crystals in avibactam or **2**. Consistent with our inhibition kinetics results, we were unable to obtain crystal structures of complexes of L1 with either of these inhibitors. L2 crystallised in the space group $P2_12_12_1$ with two molecules in the asymmetric unit (**Table S3**), and closely conserves the overall SBL fold with, for example, an RMSD to KPC-2 (PDB 2OV5) of 0.2 Å. L2 crystals formed in a reagent containing a 0.1 M racemic mixture of the amino acids glutamate, alanine, lysine and serine. The active site manifests clear F_o-F_c density into which a molecule of D-glutamate could be modelled (**Fig S4A**), indicating the D-enantiomer preferentially binds to L2. However, binding does not perturb the active site conformation compared with an un-complexed L2 crystal structure (PDB 1O7E) (**Fig S5**), preserving positioning of the hydrolytic (deacylating) water with respect to Glu166, Asn170 and Ser70 (see **Table S4** for distances), and the conformation of the conserved, catalytically important Lys73 (Meroueh *et al.*, 2005, Fonseca *et al.*, 2012, Vandavasi *et al.*, 2016). D-glutamate binds non-covalently, through interactions of its carbonyl oxygen with the backbone amides in the oxyanion hole (formed by residues Ser70 and Ser237), the C-terminal oxygen with Ser130-Oγ, and the glutamate amide with the deacylating water (**Fig. 2A**). Despite these extensive interactions, there is little inhibitory effect, with 100 mM D-glutamate reducing L2 activity by just 20% (**Fig. S6**), indicating binding is weak and the ligand can be easily displaced by substrate. The presence of D-glutamate in the active site of our L2 crystal structure is therefore a crystallisation artefact and is due to the excess of amino acid in the crystallisation buffer. D-glutamate binds differently compared with the high affinity binding (K_i = 84 pM) of the β-lactamase inhibitory protein (BLIP) to the class A β-lactamase KPC-2 (PDB 3E2K). Interestingly, BLIP binding to KPC-2 involves localisations of an L-aspartate residues at the active site, in a manner related to, but different from, D-glutamate binding to

L2, and one that does not involve interactions with the oxyanion hole (**Fig. S7**) (Hanes *et al.*, 2009).

L2:avibactam and L2:bicyclic boronate **2** co-complex structures were solved to 1.35 Å and 2.09 Å resolution, respectively, with clear F_o-F_c density indicating both inhibitors form a covalent attachment to the active site nucleophile Ser70 (**Figs S4B and S4C**). Binding by both compounds reveals no significant changes in the L2 active site in comparison with the apo or D-glutamate structures. Indeed, in both structures the deacylating water is positioned similarly to the native and D-glutamate-bound structures (**Table S4**).

The bicyclic boronate **2** binds covalently to Ser70 of L2 (**Figure 2B**) with the boron atom clearly in a tetrahedral geometry. This is also observed previously on binding of the closely related bicyclic boronate **1** to CTX-M-15 (another class A ESBL) (Cahill *et al.*, 2017) and OXA-10 (a class D SBL) (Brem *et al.*, 2016). Hence, bicyclic boronates bind SBLs in a form that mimics the first tetrahedral intermediate formed during β-lactam hydrolysis, which is involved in acyl-enzyme formation, rather than mimicking the acyl-enzyme itself, i.e. these inhibitors are 'transition state analogues'. As in D-glutamate binding, the assigned OH group on the boron atom is positioned to make strong interactions with the backbone amides of Ser70 (2.95 Å) and Ser237 (3.1 Å) in the oxyanion hole. The bicyclic boronate **2** makes additional hydrogen bonds to the side chains of the catalytically important residues Ser130 (2.77 Å to the bicyclic ring oxygen), Asn132 (3.0 Å to the benzamide oxygen), Ser237 (2.96 Å to the carboxylate) Thr235 (2.65 Å to the carboxylate), and the backbone carbonyl oxygen of Ser237 (3.1 Å to the benzamide nitrogen). In addition, binding is stabilised by significant hydrophobic interactions with His105.

Avibactam (**Figure 2C**) binds to L2 in its ring opened form, forming a carbamoyl-enzyme complex (Ehmann *et al.*, 2012) in which its six-membered ring is in a chair

conformation, a conserved feature in other structurally characterised avibactam:β-lactamase complexes (Krishnan *et al.*, 2015, King *et al.*, 2015, Lahiri *et al.*, 2015, Xu *et al.*, 2012, Lahiri *et al.*, 2013, Lahiri *et al.*, 2014). Highlighting the importance of the oxyanion hole, as with both D-glutamate and the bicyclic boronate **2**, the avibactam derived carbamoyl oxygen is positioned to make hydrogen bonds with the oxyanion hole backbone amides of Ser70 (2.75 Å) and Ser237 (2.85 Å). His105 is also involved in providing stabilising hydrophobic interactions (3.49 Å), while the carbamoyl NH interacts with the backbone carbonyl of Ser237 (3.08 Å) and the Asn132 sidechain (2.97 Å). The carbamoyl NH interactions may be relatively less important as they present in only one molecule in the asymmetric unit (chain B). The avibactam sulfate moiety interacts with the OH groups of both Thr235 (3.10 Å) and Ser130 (2.88 Å), with an additional 3.19 Å interaction with Ser237 in chain B.

β-Lactamase production is not induced by avibactam and the bicyclic boronate 2

One important consideration when deploying β-lactamase inhibitors into clinical practice is that some can interact with penicillin binding proteins and trigger β-lactamase induction pathways carried by many bacteria. L1 and L2 production in *S. maltophilia* is controlled by a transcriptional regulator, AmpR, which is responsive to β-lactam challenge via sensing β-lactam mediated perturbations in peptidoglycan breakdown and recycling (Jacobs *et al.*, 1997, Jacobs *et al.*, 1994). Hence, we tested the ability of β-lactamase inhibitors to induce β-lactamase production in *S. maltophilia*. Clavulanic acid induces L1 production (measured using meropenem hydrolysis in cell extracts) at a similar level to the positive control β-lactam cefoxitin in the *S. maltophilia* wild type strain K279a (**Fig. 3**). This observation rationalizes why clavulanic acid does not reduce the MIC of ceftazidime against *S. maltophilia* K279a (**Table 2**): induction of L1 (**Fig. 3**) overcomes inhibition of L2 (**Table 3**) because L1 can

hydrolyse ceftazidime (**Table 1**). Since L1 does not hydrolyse aztreonam (**Table 1**), however, clavulanic acid reduces the aztreonam MIC against K279a, despite its ability to induce L1 production (**Table 2, Fig. 3**). Notably, by contrast with clavulanic acid, both avibactam and the bicyclic boronate **2** reduce ceftazidime MICs against K279a (**Table 2**). This observation is explained by the important finding that neither avibactam nor **2** induces L1 to any measurable extent (**Fig. 3**), yet both inhibit L2 (**Table 3**).

Selection and characterisation of mutants which overcome the reversal of ceftazidime resistance by avibactam and the bicyclic boronate 2.

Avibactam is currently only clinically available in combination with ceftazidime. The fact that L1 induction by clavulanic acid overcomes its ability to reduce ceftazidime MICs against *S. maltophilia* (**Fig. 3, Table 2**) led us to suggest that L1/L2 hyper-producing, ceftazidime resistant strains might further mutate to be ceftazidime resistant in the presence of avibactam and the bicyclic boronate **2** by producing even more L1. To investigate this possibility, we used a K279a *ampR* mutant, M11, which is ceftazidime resistant due to L1/L2 hyper-production but where ceftazidime resistance can be reversed following treatment with avibactam or **2** at 10 $mg.L^{-1}$ (**Table 4**). We aimed to identify mutants able to grow on ceftazidime at >32 $mg.L^{-1}$ (i.e. clinically resistant, according to CLSI breakpoints (CLSI, 2015) in the presence of either avibactam or **2** at 10 $mg.L^{-1}$. Mutants were readily obtained; those selected using ceftazidime/avibactam were also resistant to ceftazidime/**2**, and *vice versa* (**Table 4**). To investigate the basis for resistance, LC-MS/MS proteomics was used to quantify changes in protein production in the two mutants. In both cases, L1 was produced at levels ~3-fold greater than in the parent strain (**Table S5, S5, Fig. 4A**). This result was confirmed by measuring L1 enzyme activity in cell extracts using meropenem as substrate (**Fig 4B**). Thus, hyper-

production of L1 can overcome the ability of these L2-specific inhibitors to rescue ceftazidime activity against a ceftazidime-resistant strain. Importantly, however, the mutants were still sensitive to the aztreonam/avibactam or aztreonam/**2** combinations (**Table 4**) as L1 cannot hydrolyse aztreonam (**Table 1**). The L1 hyper-producing phenotype, blocking reversal of ceftazidime, but not aztreonam, resistance by β-lactamase inhibitors is clearly relevant, because it is displayed by clinical isolate CI-31 (**Table 2**).

DISCUSSION

Our structural data reveal that the bicyclic boronate **2** binds to the ESBL L2 in a manner similar to that previously observed for the closely related bicyclic boronate **1** binding to the ESBL CTX-M-15. For the bicyclic boronate **2**, binding of the tetrahedral boron atom to L2 and conformation of the bicyclic fused core are all consistent with the CTX-M-15:bicyclic boronate **1** structure (Cahill *et al.*, 2017); there is only slight variation in the amide/benzamide side chain conformations (**Fig. 5A**). Furthermore, formation of the L2 carbamoyl-enzyme complex by avibactam results in a conformationally similar mode of binding compared with structurally-characterised complexes with the class A SBLs KPC-2 (PDB 4ZBE) (Krishnan *et al.*, 2015), SHV-1 (PDB 4ZAM) (Krishnan *et al.*, 2015) and CTX-M-15 (PDB 4S2I) (King *et al.*, 2015) (**Fig. 5B**), and is consistent with data indicating avibactam to be similarly effective against these enzymes (Krishnan *et al.*, 2015, Ehmann *et al.*, 2012, Stachyra *et al.*, 2009) However, some subtle differences in active-site interactions are observed (**Fig S8**). In particular, while the avibactam carbamoyl hydrogen bond with Asn132 is conserved, the weaker carbamoyl interaction with the carbonyl oxygen of L2-Ser237 is not, highlighting that such an interaction is not essential for binding. Furthermore, the avibactam sulfate moiety interaction with Thr235 is likely important as it presents in all SBLs, while interaction with Ser130 is present in KPC-

2 alone. In SHV-1:avibactam, interaction of the sulfate group with the non-conserved Arg244 essentially substitutes for the sulfate-Ser237 interaction in other SBLs (Thr237 in KPC-2). In both SHV-1:avibactam and KPC-2:avibactam the 'hydrolytic' deacylating water molecule hydrogen bonds to the avibactam carbamoyl, while this interaction is not observed with either CTX-M-15:avibactam or L2:avibactam. The avibactam-derived sulfate-bonded nitrogen is in the same conformation as in KPC-2/SHV-1:avibactam and, unlike in the CTX-M-15:avibactam complex, is directed away from the six-membered ring and distant from Ser130 (Ser130, 3.57 Å) (King *et al.*, 2015) and consequently is not primed for re-cyclization (Choi *et al.*, 2016) in which this residue is involved (**Fig. 5B**). The CTX-M-15:avibactam complex therefore remains to date as the only crystallographic evidence for avibactam reacting with an SBL in a conformation ideal for re-cyclization (King *et al.*, 2015). Thus, the rate at which the avibactam derived complex can re-cyclize to reform intact avibactam may vary between SBLs.

Even though our structural and kinetic work confirm that L2 is potently inhibited by avibactam and the bicyclic boronate **2**, we predicted failure of avibactam/ceftazidime against *S. maltophilia*. Our prediction was based on the observation that L1-hyper-producing mutants are readily obtained from *S. maltophilia* isolates (**Fig. 4**), and avibactam does not inhibit MBLs (Abboud *et al.*, 2016) . Whilst **2** inhibits subclass B1 MBLs (Brem *et al.*, 2016) , our work reveals that it does not inhibit the subclass B3 MBL, L1 (**Table 3, Fig S2**) and so **2**/ceftazidime was also overcome by L1 hyper-production (**Table 4, Fig. 4**). It may be possible to modify **2** and so generate a broader-spectrum MBL inhibitor. However, a key finding of this work is that such a modification might not be essential. Avibactam and **2** both facilitate killing of *S. maltophilia* when paired with the monobactam, aztreonam, reducing MICs to ≤ 4 mg.L^{-1} even in the pan-resistant clinical *S. maltophilia* isolate, CI-31 (**Table 2**). These data imply that aztreonam/avibactam and aztreonam/**2** may have a promising clinical future for treatment of infections caused by this most intractable of species. The fact that efflux pump over-production

does not affect aztreonam/**2** or aztreonam/avibactam activity (**Table 2**) gives even greater cause for optimism. We were interested to read, therefore, a recent clinical case report demonstrating the use of combination therapy with ceftazidime/avibactam plus aztreonam to save the life of a patient with an *S. maltophilia* infection that had failed all prior therapy (Mojica *et al.*, 2016). Our structural, kinetic and whole bacterial killing data would lead to the conclusion that ceftazidime was probably superfluous in this success, but our work indicates that ceftazidime/avibactam plus aztreonam might be routinely considered in the clinic for use against seemingly untreatable *S. maltophilia* infections whilst aztreonam/avibactam works its way through the clinical trials system. Positive results have been seen with ceftazidime/avibactam plus aztreonam against Enterobacteriaceae isolates carrying multiple β-lactamases, but the combination was not universally efficacious (Marshall *et al.*, 2017).

In many respects, because of its inability to inhibit L1, the bicyclic boronate **2** acts against *S. maltophilia* very similarly to avibactam. One potentially significant difference is that avibactam is hydrolysed by L1, but **2** retains its structural integrity (**Fig. S3**). This hydrolysis is slow, and even if L1 is hyper-produced, it is not significant enough to confer aztreonam/avibactam resistance (**Table 4**). However, there is a chance that L1 mutants might be selected with greater avibactam hydrolytic activity, reducing the degree of L2 inhibition and raising the MIC of aztreonam/avibactam into the resistant range. This observation may also be of relevance to other avibactam-like compounds in development, e.g. Relebactam (Blizzard *et al.*, 2014). In contrast, given that modification of **2** in the presence of wild-type L1 is undetectably slow, evolution to increased breakdown may require significantly more steps, potentially increasing the long-term efficacy of aztreonam/**2** as a combination to treat *S. maltophilia* infections.

In conclusion, our combined results reveal the potential of non-classical non β-lactam containing β-lactamase inhibitors, including the clinically approved compound avibactam, and

the cyclic boronates (some of which are presently in clinical trials) for treatment of *S. maltophilia*, particularly when partnered with the monobactam aztreonam, and perhaps other aztreonam-like β-lactams currently in development. Given the structural differences between avibactam, cyclic boronates, and the β-lactam based inhibitors, it would seem that there is considerable scope for the identification of new types of β-lactamase inhibitors of potential clinical utility against Gram-negative bacterial pathogens.

EXPERIMENTAL PROCEDURES

Bacterial isolates and materials

S. maltophilia clinical isolates were K279a, a well characterised isolate from Bristol, UK, or were obtained from the SENTRY antimicrobial resistance survey, as previously reported (Gould *et al.*, 2006). The ceftazidime resistant, β-lactamase hyper-producing K279a-derived mutants used were K CAZ 10 (Talfan *et al.*, 2013) and K M11 (Okazaki & Avison, 2008). Efflux-pump over-producing mutants K AMI 32 and K MOX 8 were selected using K279a as parent strain as previously described (Gould & Avison, 2006). All growth media were from Oxoid. Chemicals were from Sigma, unless otherwise stated. Avibactam was from AstraZeneca whilst cyclic boronate **2** was synthesised according to published protocols (Burns *et al.*, 2010).

Assay of β-lactamase activity in cell extracts, β-lactamase induction and β-lactam susceptibility

Cultures were grown overnight using nutrient broth and used to inoculate (1:100 dilution) 10 mL nutrient broth cultures in sealed 30 mL universal bottles. Cultures were incubated for 2 h

with shaking at 37°C before test inducers were added, or not, and culture was continued for 2 h. Cells were pelleted by centrifugation (4,000 x g, 10 min) and pellets treated with 100 µL of BugBuster (Ambion), pipetting up and down a few times before rocking for 10 min at room temperature. Cell debris and unlysed cells were pelleted by centrifugation (13,000 x g, 5 min) and the supernatant retained as a source of crude cell protein. Protein concentrations were determined using the BioRad protein assay reagent concentrate according to the manufacturer's instructions. L1 β-lactamase activity was determined using an Omega Fluostar (BMG Biotech) using meropenem as substrate in half-area 96 well UV-translucent plates (Greiner UV-Star. Bio-one) with 200 µL of 100 µM meropenem solution in assay buffer (60 mM $Na_2HPO_4 \cdot 7H_2O$ pH 7.0, 40 mM $NaH_2PO_4 \cdot H_2O$, 10 mM KCl, 1 mM $MgSO_4 \cdot 7H_2O$, 100 µM $ZnCl_2$) plus 10 µL of cell extract. Substrate depletion was followed at 300 nm for 10 mins and an extinction coefficient of 9600 $AU.M^{-1}.cm^{-1}$ was used to calculate enzyme activity in the linear phase of the reaction.

Susceptibility to β-lactams in bacterial isolates was determined using the CLSI microtitre MIC methodology with Muller-Hinton Broth using 96 well plates (Corning, Costar). The MIC was determined as the lowest concentration of β-lactam required to entirely suppress growth (CLSI, 2015). Inhibitor concentrations were kept constant at 2 $mg.L^{-1}$ or 10 $mg.L^{-1}$ in all assays. Interpretation of susceptibility/resistance was by reference to CLSI clinical breakpoints for *S. maltophilia* (ceftazidime) and for *Pseudomonas aeruginosa* (for aztreonam and meropenem, since no *S. maltophilia* breakpoints are available) (CLSI, 2015).

Proteomic Analysis

Cells in 50 mL nutrient broth cultures were pelleted by centrifugation (10 min, 4,000 × g, 4˚C) and resuspended in 20 mL of 30 mM Tris-HCl, pH 8 and broken by sonication using a cycle

of 1 sec on, 0.5 sec off for 3 min at amplitude of 63% using a Sonics Vibracell VC-505TM (Sonics and Materials Inc., Newton, Connecticut, USA). The sonicated samples were centrifuged at 8,000 rpm (Sorval RC5B PLUS using an SS-34 rotor) for 15 min at 4˚C to pellet intact cells and large cell debris; the supernatant was removed and concentrated (Amicon 3 kDa cutoff filter) for analysis of total cell protein. Alternatively, for envelope preparations, the supernatant was not concentrated, and instead, subjected to centrifugation at 20,000 rpm for 60 min at 4˚C using the above rotor to pellet total envelopes. To isolate total envelope proteins, this total envelope pellet was solubilised using 200 µL of 30 mM Tris-HCl pH 8 containing 0.5% (w/v) SDS.

Protein concentrations in all samples was quantified using Biorad Protein Assay Dye Reagent Concentrate according to the manufacturer's instructions. Proteins (2.5 µg/Lane for total cell proteomics or 5 µg/Lane for envelope protein analysis) were separated by SDS-PAGE using 11% acrylamide, 0.5% bis-acrylamide (Biorad) gels and a Biorad Min-Protein Tetracell chamber model 3000X1. Gels were resolved at 200 V until the dye front had moved approximately 1 cm into the separating gel. Proteins in all gels were stained with Instant Blue (Expedeon) for 20 min and de-stained in water.

The 1 cm of gel lane was subjected to in-gel tryptic digestion using a DigestPro automated digestion unit (Intavis Ltd). The resulting peptides from each gel fragment were fractionated separately using an Ultimate 3000 nanoHPLC system in line with an LTQ-Orbitrap Velos mass spectrometer (Thermo Scientific). In brief, peptides in 1% (v/v) formic acid were injected onto an Acclaim PepMap C18 nano-trap column (Thermo Scientific). After washing with 0.5% (v/v) acetonitrile plus 0.1% (v/v) formic acid, peptides were resolved on a 250 mm × 75 µm Acclaim PepMap C18 reverse phase analytical column (Thermo Scientific) over a 150 min organic gradient, using 7 gradient segments (1-6% solvent B over 1 min., 6-15% B over 58 min., 15-32% B over 58 min., 32-40% B over 5 min., 40-90% B over 1 min.,

held at 90% B for 6 min and then reduced to 1% B over 1 min.) with a flow rate of 300 nL/min. Solvent A was 0.1% formic acid and Solvent B was aqueous 80% acetonitrile in 0.1% formic acid. Peptides were ionized by nano-electrospray ionization MS at 2.1 kV using a stainless-steel emitter with an internal diameter of 30 μm (Thermo Scientific) and a capillary temperature of 250°C. Tandem mass spectra were acquired using an LTQ-Orbitrap Velos mass spectrometer controlled by Xcalibur 2.1 software (Thermo Scientific) and operated in data-dependent acquisition mode. The Orbitrap was set to analyze the survey scans at 60,000 resolution (at m/z 400) in the mass range m/z 300 to 2000 and the top twenty multiply charged ions in each duty cycle selected for MS/MS in the LTQ linear ion trap. Charge state filtering, where unassigned precursor ions were not selected for fragmentation, and dynamic exclusion (repeat count, 1; repeat duration, 30 s; exclusion list size, 500) were used. Fragmentation conditions in the LTQ were as follows: normalized collision energy, 40%; activation q, 0.25; activation time 10 ms; and minimum ion selection intensity, 500 counts.

The raw data files were processed and quantified using Proteome Discoverer software v1.4 (Thermo Scientific) and searched against the UniProt *S. maltophilia* strain K279a database (4365 protein entries; UniProt accession UP000008840) using the SEQUEST (Ver. 28 Rev. 13) algorithm. Peptide precursor mass tolerance was set at 10 ppm, and MS/MS tolerance was set at 0.8 Da. Search criteria included carbamidomethylation of cysteine (+57.0214) as a fixed modification and oxidation of methionine (+15.9949) as a variable modification. Searches were performed with full tryptic digestion and a maximum of 1 missed cleavage was allowed. The reverse database search option was enabled and all peptide data was filtered to satisfy false discovery rate (FDR) of 5 %. The Proteome Discoverer software generates a reverse “decoy” database from the same protein database used for the analysis and any peptides passing the initial filtering parameters that were derived from this decoy database are defined as false positive identifications. The minimum cross-correlation factor filter was readjusted for each

individual charge state separately to optimally meet the predetermined target FDR of 5 % based on the number of random false positive matches from the reverse decoy database. Thus, each data set has its own passing parameters. Protein abundance measurements were calculated from peptide peak areas using the Top 3 method (Silva *et al.*, 2006) and proteins with fewer than three peptides identified were excluded. The proteomic analysis was repeated three times for each parent and mutant strain, each using a separate batch of cells. Data analysis was as follows: all raw protein abundance data were uploaded into Microsoft Excel. Raw data from each sample were normalised by division by the average abundance of all 30S and 50S ribosomal protein in that sample. A one-tailed, unpaired T-test was used to calculate the significance of any difference in normalised protein abundance data in the three sets of data from the parent strains versus the three sets of data from the mutant derivative. A p-value of <0.05 was considered significant. The fold change in abundance for each protein in the mutant compared to its parent was calculated using the averages of normalised protein abundance data for the three biological replicates for each strain. All raw protein abundance data are provided in the attached proteomics data file.

Purification of L1 and L2 and kinetics assays

Recombinant L1 and L2 proteins were produced in *E. coli* and purified as previously described (Calvopina *et al.*, 2016). Enzyme activity was monitored using an Omega Fluostar (BMG Labtech) using buffer L1 (50 mM HEPES pH 7.5, 10 µg.mL^{-1} BSA, 10 µM $ZnSO_4$ and 0.01% v/v Triton X-100) and buffer L2 (50 mM Tris pH 7.5, 10 µg.mL^{-1} BSA and 0.01% v/v Triton X-100). Reactions were carried out as described in (van Berkel *et al.*, 2013). For the chromogenic substrates meropenem, ceftazidime and aztreonam, substrate depletion was measured at 300 nm, 260 nm, 318 nm, respectively whilst for the fluorogenic substrate FC5,

the excitation wavelength was set at 380nm and emission wavelength at 460 nm (van Berkel *et al.*, 2013). Clavulanic acid was dissolved in double distilled water while avibactam and the bicyclic boronate **2** were dissolved in DMSO to prepare an appropriate stock solution. IC_{50} values were calculated from reactions using FC5 (50 nM) as substrate for both L1 and L2 (used at 50 pM). Steady state kinetic data were analysed by curve fitting to the Michaelis-Menten equation using Prism software.

L2 Crystallisation, Data Collection and Structure Modelling

Initial L2 crystals grew using sitting-drop vapour diffusion in 96-well MRC 2-drop plates (Molecular Dimensions) with the Morpheus sparse matrix screen (Gorrec, 2009). Conditions were refined in CrysChem 24-well sitting-drop plates (Hampton Research, 18 °C), and diffraction-quality crystals were obtained by mixing 1 µL of L2 protein (42 $mg.mL^{-1}$) with 1.5 µL reagent (10% w/v PEG 20000, 20% v/v PEG MME 550, 0.02 M DL-Glutamic acid; 0.02 M DL-Alanine; 0.02 M Glycine; 0.02 M DL-Lysine; 0.02 M DL-Serine, 0.1 M bicine/Trizma base pH 8.5) and equilibrated against 500 µL reagent. L2 complexes were obtained by soaking crystals in bicyclic boronate **2** (5 min, 2.5 mM) or avibactam (40 min, 5 mM) dissolved in reservoir reagent. L2 crystals were cryoprotected using reservoir solution plus 20% glycerol and flash frozen in liquid nitrogen. Crystallographic data were collected at 100K (I04-1, I04 or I03, Diamond Light Source, UK) and integrated in XDS (Kabsch, 2010) or DIALS (Waterman *et al.*, 2016), and scaled in Aimless in the CCP4 suite (Winn *et al.*, 2011). Phases were calculated by molecular replacement in Phaser (McCoy *et al.*, 2007) using PDB 1O7E (unpublished) as a starting model. Avibactam and boronate structures, covalently bound to Ser70, and geometric restraints were generated using Phenix eLBOW (Moriarty *et al.*, 2009). Structures were completed by iterative rounds of manual model building in Coot (Emsley *et*

al., 2010) and refinement in Phenix (Adams *et al.*, 2010). Structure validation was assisted by Molprobity (Chen *et al.*, 2010) and Phenix (Adams *et al.*, 2010). Figures were prepared using Pymol (Schrodinger).

NMR Spectroscopy

The potential impact of avibactam or the bicyclic boronate **2** (both 75 μM) on the hydrolysis of meropenem (1 mM) by L1 (75 nM) was monitored over 20 min. The hydrolysis of avibactam (400 μM) and **2** (400 μM) by L1 (10 μM) was monitored over the course of 18 h or 24 h, respectively. All substrates, inhibitors, and enzymes were prepared in 50 mM Tris-d_{11}, pH 7.5, 10 % D_2O. Spectra were acquired on a Bruker AVIII 700 MHz spectrometer equipped with a $^{1}H/^{13}C/^{15}N$ TCI cryoprobe, and a Bruker AVIIIHD 600 MHz spectrometer equipped with a Prodigy broadband cryoprobe. ^{1}H spectra were acquired at 298 K using a 2 s relaxation delay, and were processed with a 0.3 Hz line broadening. The water signal was suppressed by excitation sculpting with perfect echo.

ACKNOWLEDGEMENTS

This work was funded, in part, by grants MR/N013646/1 to M.B.A & K.J.H, EP/M027546/1 to M.B.A & J.S and MR/N002679/1 to C.J.S. from the Antimicrobial Resistance Cross Council Initiative supported by the seven United Kingdom research councils. Additional funding was provided by grants from the National Institute of Allergy and Infectious Diseases of the U.S. National Institutes of Health (R01AI100560) to J.S and from the United Kingdom Medical Research Council and the Canadian Institute for Health Research (G1100135) to J.S.

C.J.S. and C.W.G.F. K.C. was in receipt of a postgraduate scholarship from SENESCYT, Ecuador. We thank Diamond Light Source for access to beamlines I03, I04 and I04-1 (proposal number MX12342) that contributed to the results presented here, and the staff of the Diamond macromolecular crystallography village for their help.

DATA AVAILABILITY

Coordinates and structure factors for L2:native, L2:avibactam and L2:cyclic boronate **2** have been deposited in the Protein Data Bank under accession codes 5NE2, 5NE3 and 5NE1, respectively.

AUTHOR CONTRIBUTIONS

Conception and design: MBA, JS, CJS, CGWF, PH, JB.

Acquisition of data: KC, PH, JB, KJH, SJ, RC, CTL.

Analysis and Interpretation of data: ALL AUTHORS.

Drafting the manuscript; ALL AUTHORS.

CONFLICTS OF INTEREST

The authors declare that they have no conflict of interest.

REFERENCES

Abboud, M.I., C. Damblon, J. Brem, N. Smargiasso, P. Mercuri, B. Gilbert, A.M. Rydzik, T.D.W. Claridge, C.J. Schofield & J.M. Frere, (2016) Interaction of Avibactam with Class B Metallo-beta-Lactamases. *Antimicrob Agents Ch* **60**: 5655-5662.

Adams, P.D., P.V. Afonine, G. Bunkoczi, V.B. Chen, I.W. Davis, N. Echols, J.J. Headd, L.-W. Hung, G.J. Kapral, R.W. Grosse-Kunstleve, A.J. McCoy, N.W. Moriarty, R. Oeffner, R.J. Read, D.C. Richardson, J.S. Richardson, T.C. Terwilliger & P.H. Zwart, (2010) PHENIX: a comprehensive Python-based system for macromolecular structure solution. *Acta Crystallographica Section D* **66**: 213-221.

Al Roomi, L.G., A.M. Sutton, F. Cockburn & T.A. McAllister, (1984) Amoxycillin and clavulanic acid in the treatment of urinary infection. *Archives of Disease in Childhood* **59**: 256-259.

Alonso, A. & J.L. Martinez, (2000) Cloning and characterization of SmeDEF, a novel multidrug efflux pump from *Stenotrophomonas maltophilia*. *Antimicrob Agents Chemother* **44**: 3079-3086.

Ambler, R.P., (1980) The Structure of β-Lactamases. *Philosophical Transactions of the Royal Society of London. B, Biological Sciences* **289**: 321.

Blizzard, T.A., H. Chen, S. Kim, J. Wu, R. Bodner, C. Gude, J. Imbriglio, K. Young, Y.-W. Park, A. Ogawa, S. Raghoobar, N. Hairston, R.E. Painter, D. Wisniewski, G. Scapin, P. Fitzgerald, N. Sharma, J. Lu, S. Ha, J. Hermes & M.L. Hammond, (2014) Discovery of MK-7655, a β-lactamase inhibitor for combination with Primaxin®. *Bioorganic & Medicinal Chemistry Letters* **24**: 780-785.

Brem, J., R. Cain, S. Cahill, M.A. McDonough, I.J. Clifton, J.C. Jimenez-Castellanos, M.B. Avison, J. Spencer, C.W.G. Fishwick & C.J. Schofield, (2016) Structural basis of metallo-beta-lactamase, serine-beta-lactamase and penicillin-binding protein inhibition by cyclic boronates. *Nat Commun* **7**.

Brooke, J.S., (2012) *Stenotrophomonas maltophilia*: an Emerging Global Opportunistic Pathogen. *Clinical Microbiology Reviews* **25**: 2-41.

Burns, C.J., R. Goswami, R.W. Jackson, T. Lessen, W. Li, D. Pevear, P.K. Tirunahari & H. Xu, (2010) Beta-lactamase inhibitors. In.: Google Patents, pp.

Bush, K., (2013) The ABCD's of β-lactamase nomenclature. *Journal of Infection and Chemotherapy* **19**: 549-559.

Cahill, S.T., R. Cain, D.Y. Wang, C.T. Lohans, D.W. Wareham, H.P. Oswin, J. Mohammed, J. Spencer, C.W. Fishwick, M.A. McDonough, C.J. Schofield & J. Brem, (2017) Cyclic Boronates Inhibit All Classes of beta-Lactamase. *Antimicrob Agents Chemother*.

Calvopina, K., K.D. Umland, A.M. Rydzik, P. Hinchliffe, J. Brem, J. Spencer, C.J. Schofield & M.B. Avison, (2016) Sideromimic Modification of Lactivicin Dramatically Increases Potency against Extensively Drug-Resistant *Stenotrophomonas maltophilia* Clinical Isolates. *Antimicrob Agents Chemother* **60**: 4170-4175.

Chen, V.B., W.B. Arendall, III, J.J. Headd, D.A. Keedy, R.M. Immormino, G.J. Kapral, L.W. Murray, J.S. Richardson & D.C. Richardson, (2010) MolProbity: all-atom structure validation for macromolecular crystallography. *Acta Crystallographica Section D* **66**: 12-21.

Choi, H., R.S. Paton, H. Park & C.J. Schofield, (2016) Investigations on recyclisation and hydrolysis in avibactam mediated serine β-lactamase inhibition. *Organic & Biomolecular Chemistry* **14**: 4116-4128.

ClinicalTrials.gov, (2016) VNRX-5133-101/102: A Randomized, Double Blind, Placebo-Controlled, Sequential Group, Dose-Escalation Study to Evaluate the Safety, Tolerability, and Pharmacokinetics of Single and Repeat Doses of VNRX-5133 in Healthy Adult Volunteers. In., pp.

CLSI, (2015) Performance Standards for Antimicrobial Susceptibility Testing; Twenty-Fifth Informational Supplement. *Wayne, PA: Clinical and Laboratory Standards Institute* **CLSI document M100-S25**.

Coleman, K., (2011) Diazabicyclooctanes (DBOs): a potent new class of non-β-lactam β-lactamase inhibitors. *Current Opinion in Microbiology* **14**: 550-555.

Crossman, L.C., V.C. Gould, J.M. Dow, G.S. Vernikos, A. Okazaki, M. Sebaihia, D. Saunders, C. Arrowsmith, T. Carver, N. Peters, E. Adlem, A. Kerhornou, A. Lord, L. Murphy, K. Seeger, R. Squares, S. Rutter, M.A. Quail, M.-A. Rajandream, D. Harris, C. Churcher, S.D. Bentley, J. Parkhill, N.R. Thomson & M.B. Avison, (2008) The complete genome, comparative and functional analysis of *Stenotrophomonas maltophilia* reveals an organism heavily shielded by drug resistance determinants. *Genome Biology* **9**: R74-R74.

de Vrankrijker, A.M.M., T.F.W. Wolfs & C.K. van der Ent, (2010) Challenging and emerging pathogens in cystic fibrosis. *Paediatric Respiratory Reviews* **11**: 246-254.

Drawz, S.M. & R.A. Bonomo, (2010) Three Decades of β-Lactamase Inhibitors. *Clinical Microbiology Reviews* **23**: 160-201.

Drawz, S.M., K.M. Papp-Wallace & R.A. Bonomo, (2014) New beta-Lactamase Inhibitors: a Therapeutic Renaissance in an MDR World. *Antimicrob Agents Ch* **58**: 1835-1846.

Ehmann, D.E., H. Jahić, P.L. Ross, R.-F. Gu, J. Hu, G. Kern, G.K. Walkup & S.L. Fisher, (2012) Avibactam is a covalent, reversible, non–β-lactam β-lactamase inhibitor. *Proceedings of the National Academy of Sciences* **109**: 11663-11668.

Emsley, P., B. Lohkamp, W.G. Scott & K. Cowtan, (2010) Features and development of Coot. *Acta Crystallographica Section D* **66**: 486-501.

Fass, R.J. & R.B. Prior, (1989) Comparative in vitro activities of piperacillin-tazobactam and ticarcillin-clavulanate. *Antimicrob Agents Ch* **33**: 1268-1274.

Finlay, J., L. Miller & J.A. Poupard, (2003) A review of the antimicrobial activity of clavulanate. *Journal of Antimicrobial Chemotherapy* **52**: 18-23.

Fonseca, F., E.I. Chudyk, M.W. van der Kamp, A. Correia, A.J. Mulholland & J. Spencer, (2012) The Basis for Carbapenem Hydrolysis by Class A β-Lactamases: A Combined Investigation using Crystallography and Simulations. *Journal of the American Chemical Society* **134**: 18275-18285.

Garcia-Leon, G., C.R.D. Puig, C.G. de la Fuente, L. Martinez-Martinez, J.L. Martinez & M.B. Sanchez, (2015) High-level quinolone resistance is associated with the overexpression of *smeVWX* in *Stenotrophomonas maltophilia* clinical isolates. *Clin Microbiol Infec* **21**: 464-467.

Gorrec, F., (2009) The MORPHEUS protein crystallization screen. *Journal of Applied Crystallography* **42**: 1035-1042.

Gould, V.C. & M.B. Avison, (2006) SmeDEF-mediated antimicrobial drug resistance in *Stenotrophomonas maltophilia* clinical isolates having defined phylogenetic relationships. *J Antimicrob Chemother* **57**: 1070-1076.

Gould, V.C., A. Okazaki & M.B. Avison, (2006) Beta-lactam resistance and beta-lactamase expression in clinical *Stenotrophomonas maltophilia* isolates having defined phylogenetic relationships. *J Antimicrob Chemother* **57**: 199-203.

Gould, V.C., A. Okazaki & M.B. Avison, (2013) Coordinate hyperproduction of SmeZ and SmeJK efflux pumps extends drug resistance in *Stenotrophomonas maltophilia*. *Antimicrob Agents Chemother* **57**: 655-657.

Hamad, B., (2010) The antibiotics market. *Nat Rev Drug Discov* **9**: 675-676.

Hanes, M.S., K.M. Jude, J.M. Berger, R.A. Bonomo & T.M. Handel, (2009) Structural and Biochemical Characterization of the Interaction between KPC-2 β-Lactamase and β-Lactamase Inhibitor Protein. *Biochemistry* **48**: 9185-9193.

Hecker, S.J., K.R. Reddy, M. Totrov, G.C. Hirst, O. Lomovskaya, D.C. Griffith, P. King, R. Tsivkovski, D. Sun, M. Sabet, Z. Tarazi, M.C. Clifton, K. Atkins, A. Raymond, K.T. Potts, J. Abendroth, S.H. Boyer, J.S. Loutit, E.E. Morgan, S. Durso & M.N. Dudley, (2015) Discovery of a Cyclic Boronic Acid β-Lactamase Inhibitor (RPX7009) with Utility vs Class A Serine Carbapenemases. *Journal of Medicinal Chemistry* **58**: 3682-3692.

Huang, Y.W., C.W. Lin, H.C. Ning, Y.T. Lin, Y.C. Chang & T.C. Yang, (2017) Overexpression of SmeDEF Efflux Pump Decreases Aminoglycoside Resistance in *Stenotrophomonas maltophilia*. *Antimicrob Agents Chemother*.

Jacobs, C., J.-M. Frère & S. Normark, (1997) Cytosolic Intermediates for Cell Wall Biosynthesis and Degradation Control Inducible β-Lactam Resistance in Gram-Negative Bacteria. *Cell* **88**: 823-832.

Jacobs, C., L.J. Huang, E. Bartowsky, S. Normark & J.T. Park, (1994) Bacterial cell wall recycling provides cytosolic muropeptides as effectors for beta-lactamase induction. *The EMBO Journal* **13**: 4684-4694.

Kabsch, W., (2010) XDS. *Acta Crystallographica Section D* **66**: 125-132.

King, A.M., D.T. King, S. French, E. Brouillette, A. Asli, J.A.N. Alexander, M. Vuckovic, S.N. Maiti, T.R. Parr, E.D. Brown, F. Malouin, N.C.J. Strynadka & G.D. Wright, (2016) Structural and Kinetic Characterization of Diazabicyclooctanes as Dual Inhibitors of Both Serine-β-Lactamases and Penicillin-Binding Proteins. *ACS Chemical Biology* **11**: 864-868.

King, D.T., A.M. King, S.M. Lal, G.D. Wright & N.C.J. Strynadka, (2015) Molecular Mechanism of Avibactam-Mediated beta-Lactamase Inhibition. *Acs Infect Dis* **1**: 175-184.

Krishnan, N.P., N.Q. Nguyen, K.M. Papp-Wallace, R.A. Bonomo & F. van den Akker, (2015) Inhibition of Klebsiella beta-Lactamases (SHV-1 and KPC-2) by Avibactam: A Structural Study. *Plos One* **10**.

Lahiri, S.D., M.R. Johnstone, P.L. Ross, R.E. McLaughlin, N.B. Olivier & R.A. Alm, (2014) Avibactam and Class C beta-Lactamases: Mechanism of Inhibition, Conservation of the Binding Pocket, and Implications for Resistance. *Antimicrob Agents Ch* **58**: 5704-5713.

Lahiri, S.D., S. Mangani, T. Durand-Reville, M. Benvenuti, F. De Luca, G. Sanyal & J.D. Docquier, (2013) Structural Insight into Potent Broad-Spectrum Inhibition with Reversible Recyclization Mechanism: Avibactam in Complex with CTX-M-15 and Pseudomonas aeruginosa AmpC beta-Lactamases. *Antimicrob Agents Ch* **57**: 2496-2505.

Lahiri, S.D., S. Mangani, H. Jahic, M. Benvenuti, T.F. Durand-Reville, F. De Luca, D.E. Ehmann, G.M. Rossolini, R.A. Alm & J.D. Docquier, (2015) Molecular Basis of Selective Inhibition and Slow Reversibility of Avibactam against Class D Carbapenemases: A Structure-Guided Study of OXA-24 and OXA-48. *Acs Chemical Biology* **10**: 591-600.

Lemmen, S.W., H. Häfner, R.R. Reinert, D. Zolldann, K. Kümmerer & R. Lütticken, (2001) Comparison of serum bactericidal activity of ceftazidime, ciprofloxacin and meropenem against *Stenotrophomonas maltophilia*. *Journal of Antimicrobial Chemotherapy* **47**: 118-120.

Looney, W.J., M. Narita & K. Muhlemann, (2009) *Stenotrophomonas maltophilia*: an emerging opportunist human pathogen. *Lancet Infect Dis* **9**: 312-323.

Marshall, S., A.M. Hujer, L.J. Rojas, K.M. Papp-Wallace, R.M. Humphries, B. Spellberg, K.M. Hujer, E.K. Marshall, S.D. Rudin, F. Perez, B.M. Wilson, R.B. Wasserman, L. Chikowski, D.L. Paterson, A.J. Vila, D. van Duin, B.N. Kreiswirth, H.F. Chambers, V.G. Fowler, M.R. Jacobs, M.E. Pulse, W.J. Weiss & R.A. Bonomo, (2017) Can Ceftazidime-Avibactam and Aztreonam Overcome beta-Lactam Resistance Conferred by Metallo-beta-Lactamases in Enterobacteriaceae? *Antimicrob Agents Ch* **61**.

McCoy, A.J., R.W. Grosse-Kunstleve, P.D. Adams, M.D. Winn, L.C. Storoni & R.J. Read, (2007) Phaser crystallographic software. *Journal of Applied Crystallography* **40**: 658-674.

Meroueh, S.O., J.F. Fisher, H.B. Schlegel & S. Mobashery, (2005) Ab Initio QM/MM Study of Class A β-Lactamase Acylation: Dual Participation of Glu166 and Lys73 in a Concerted Base Promotion of Ser70. *Journal of the American Chemical Society* **127**: 15397-15407.

Mojica, M.F., C.P. Ouellette, A. Leber, M.B. Becknell, M.I. Ardura, F. Perez, M. Shimamura, R.A. Bonomo, S.L. Aitken & S.A. Shelburne, (2016) Successful Treatment of Bloodstream Infection Due to Metallo-β-Lactamase-Producing Stenotrophomonas maltophilia in a Renal Transplant Patient. *Antimicrob Agents Ch* **60**: 5130-5134.

Moriarty, N.W., R.W. Grosse-Kunstleve & P.D. Adams, (2009) electronic Ligand Builder and Optimization Workbench (eLBOW): a tool for ligand coordinate and restraint generation. *Acta Crystallographica Section D* **65**: 1074-1080.

Okazaki, A. & M.B. Avison, (2008) Induction of L1 and L2 beta-lactamase production in *Stenotrophomonas maltophilia* is dependent on an AmpR-type regulator. *Antimicrob Agents Chemother* **52**: 1525-1528.

Reading, C. & M. Cole, (1977) Clavulanic Acid: a Beta-Lactamase-Inhibiting Beta-Lactam from Streptomyces clavuligerus. *Antimicrob Agents Ch* **11**: 852-857.

Ryan, R.P., S. Monchy, M. Cardinale, S. Taghavi, L. Crossman, M.B. Avison, G. Berg, D. van der Lelie & J.M. Dow, (2009) The versatility and adaptation of bacteria from the genus *Stenotrophomonas*. *Nat Rev Micro* **7**: 514-525.

Silva, J.C., M.V. Gorenstein, G.Z. Li, J.P. Vissers & S.J. Geromanos, (2006) Absolute quantification of proteins by LCMSE: a virtue of parallel MS acquisition. *Mol Cell Proteomics* **5**: 144-156.

Stachyra, T., P. Levasseur, M.-C. Péchereau, A.-M. Girard, M. Claudon, C. Miossec & M.T. Black, (2009) In vitro activity of the β-lactamase inhibitor NXL104 against KPC-2 carbapenemase and Enterobacteriaceae expressing KPC carbapenemases. *Journal of Antimicrobial Chemotherapy* **64**: 326-329.

Stachyra, T., M.C. Pechereau, J.M. Bruneau, M. Claudon, J.M. Frere, C. Miossec, K. Coleman & M.T. Black, (2010) Mechanistic studies of the inactivation of TEM-1 and P99 by NXL104, a novel non-beta-lactam beta-lactamase inhibitor. *Antimicrob Agents Chemother* **54**: 5132-5138.

Strynadka, N.C.J., H. Adachi, S.E. Jensen, K. Johns, A. Sielecki, C. Betzel, K. Sutoh & M.N.G. James, (1992) Molecular structure of the acyl-enzyme intermediate in [beta]-lactam hydrolysis at 1.7 A resolution. *Nature* **359**: 700-705.

Sulton, D., D. Pagan-Rodriguez, X. Zhou, Y.D. Liu, A.M. Hujer, C.R. Bethel, M.S. Helfand, J.M. Thomson, V.E. Anderson, J.D. Buynak, L.M. Ng & R.A. Bonomo, (2005) Clavulanic acid inactivation of SHV-1 and the inhibitor-resistant S130G SHV-1 beta-lactamase - Insights into the mechanism of inhibition. *J Biol Chem* **280**: 35528-35536.

Talfan, A., O. Mounsey, M. Charman, E. Townsend & M.B. Avison, (2013) Involvement of mutation in *ampD* I, *mrcA*, and at least one additional gene in beta-lactamase hyperproduction in *Stenotrophomonas maltophilia*. *Antimicrob Agents Chemother* **57**: 5486-5491.

van Berkel, S.S., J. Brem, A.M. Rydzik, R. Salimraj, R. Cain, A. Verma, R.J. Owens, C.W.G. Fishwick, J. Spencer & C.J. Schofield, (2013) Assay Platform for Clinically Relevant Metallo-β-lactamases. *Journal of Medicinal Chemistry* **56**: 6945-6953.

Van Boeckel, T.P., S. Gandra, A. Ashok, Q. Caudron, B.T. Grenfell, S.A. Levin & R. Laxminarayan, Global antibiotic consumption 2000 to 2010: an analysis of national pharmaceutical sales data. *The Lancet Infectious Diseases* **14**: 742-750.

Vandavasi, V.G., K.L. Weiss, J.B. Cooper, P.T. Erskine, S.J. Tomanicek, A. Ostermann, T.E. Schrader, S.L. Ginell & L. Coates, (2016) Exploring the Mechanism of β-Lactam Ring Protonation in the Class A β-lactamase Acylation Mechanism Using Neutron and X-ray Crystallography. *Journal of Medicinal Chemistry* **59**: 474-479.

Versporten, A., G. Bolokhovets, L. Ghazaryan, V. Abilova, G. Pyshnik, T. Spasojevic, I. Korinteli, L. Raka, B. Kambaralieva, L. Cizmovic, A. Carp, V. Radonjic, N. Maqsudova, H.D. Celik, M. Payerl-Pal, H.B. Pedersen, N. Sautenkova, H. Goossens & W.E.-E.P. Grp, (2014) Antibiotic use in eastern Europe: a cross-national database study in coordination with the WHO Regional Office for Europe. *Lancet Infect Dis* **14**: 381-387.

Walsh, T.R., L. Hall, S.J. Assinder, W.W. Nichols, S.J. Cartwright, A.P. Macgowan & P.M. Bennett, (1994) Sequence-Analysis of the L1 Metallo-Beta-Lactamase from *Xanthomonas maltophilia*. *BBA-Gene Struct Expr* **1218**: 199-201.

Walsh, T.R., A.P. MacGowan & P.M. Bennett, (1997) Sequence analysis and enzyme kinetics of the L2 serine beta-lactamase from *Stenotrophomonas maltophilia*. *Antimicrob Agents Ch* **41**: 1460-1464.

Wang, D.Y., M.I. Abboud, M.S. Markoulides, J. Brem & C.J. Schofield, (2016) The road to avibactam: the first clinically useful non-beta-lactam working somewhat like a beta-lactam. *Future Med Chem* **8**: 1063-1084.

Waterman, D.G., G. Winter, R.J. Gildea, J.M. Parkhurst, A.S. Brewster, N.K. Sauter & G. Evans, (2016) Diffraction-geometry refinement in the DIALS framework. *Acta Crystallographica Section D* **72**: 558-575.

Winn, M.D., C.C. Ballard, K.D. Cowtan, E.J. Dodson, P. Emsley, P.R. Evans, R.M. Keegan, E.B. Krissinel, A.G.W. Leslie, A. McCoy, S.J. McNicholas, G.N. Murshudov, N.S. Pannu, E.A. Potterton, H.R. Powell, R.J. Read, A. Vagin & K.S. Wilson, (2011) Overview of the CCP4 suite and current developments. *Acta Crystallographica Section D: Biological Crystallography* **67**: 235-242.

Xu, H., S. Hazra & J.S. Blanchard, (2012) NXL104 Irreversibly Inhibits the beta-Lactamase from *Mycobacterium tuberculosis*. *Biochemistry* **51**: 4551-4557.

TABLES

Table 1, Kinetic data for β-lactams tested against metallo L1 and serine L2 *S. maltophilia* β-lactamases.

Enzyme	**Substrate**	**[E] (μM)**	K_M **(μM)**	k_{cat} **(s^{-1})**	k_{cat}/K_M **($M^{-1}.s^{-1}$) x10^{-9}**
L1	Ceftazidime	0.5	260	1.7	6.5
	Aztreonam	0.5	-	-	-
	Meropenem	0.01	110	24	220
	FC5	0.05	30	150	5,000
L2	Ceftazidime	0.5	550	1.9	3.5
	Aztreonam	0.5	120	0.08	0.67
	Meropenem	0.625	29	0.03	1.0
	FC5	0.05	18	210	12,000

Table 2. Minimum Inhibitory Concentrations (mg.L^{-1}) of β-lactams against *S. maltophilia* in the presence of β-lactamase inhibitors used at 2 mg.L^{-1}.

	Ceftazidime				Aztreonam				Meropenem			
	-	+CLA	+BOR	+AVI	-	+CLA	+BOR	+AVI	-	+CLA	+BOR	+AVI
K279a	4	4	0.5	1	128	1	1	1	8	32	4	16
CI-20	16	16	2	4	128	4	2	2	64	32	8	64
CI-29	8	4	0.5	1	128	1	1	1	32	16	8	32
K CAZ 10	64	8	4	8	256	0.5	1	1	64	8	16	64
CI-31	256	128	128	128	256	2	4	4	256	256	256	256
K AMI 32	2	1	1	0.5	128	0.5	1	0.5	4	8	4	16
K MOX 8	4	1	0.5	0.5	128	0.25	1	0.5	4	8	8	16

Shaded values indicate clinically relevant resistance according to CLSI breakpoints (CLSI, 2015)

CLA, clavulanic acid; BOR, bicyclic boronate **2**; AVI, avibactam

Table 3. Inhibition of L2 by β-lactamase inhibitors *in vitro*.

Inhibitor	**IC_{50} (nM)**	**pIC_{50}**
Clavulanic Acid	22.3	7.41
Avibactam	14.36	7.84
Bicyclic Boronate **2**	5.25	8.27

Table 4 MICs (mg.L^{-1}) of β-lactams against *S. maltophilia* mutants in the presence of β-lactamase inhibitor (10 mg.L^{-1}).

	Ceftazidime			Aztreonam		
	-	+BOR	+AVI	-	+BOR	+AVI
K279a	4	0.5	1	128	1	1
M11	128	8	2	256	1	1
MA27	256	32	32	256	4	4
MB25	256	64	128	256	4	4

Shaded values represent resistance according to CLSI breakpoints.

BOR, bicyclic boronate **2**; AVI, avibactam.

MA27 and MB25 were selected for growth at 32 mg.L^{-1} ceftazidime in the presence of 10 mg.L^{-1} avibactam or bicyclic boronate **2**, respectively using M11 as parent strain. M11 is an L1/L2 hyper-producing mutant derived from K279a, which is wild-type [37].

FIGURE LEGENDS

Figure 1. Chemical structures of β-lactamase inhibitors.

Top, clavulanic acid. Middle, avibactam and the acyl-enzyme complex formed on the (potentially reversible) reaction of avibactam with Serine β-lactamases. Bottom, left: the monocyclic boronate, vaborbactam; right: bicyclic boronate **2**.

Figure 2. Interaction of β-lactamase inhibitors with the L2 active site.

View of L2 (shown in green cartoon) active sites with bound ligands (blue sticks), (A) D-glutamate, (B) bicyclic boronate **2** and (C) avibactam. Interactions between residues and the catalytic water are shown as red dashes, and interactions between residues and ligand as blue dashes. Labelled residues are those that specifically interact with the ligand.

Figure 3. L1 β-lactamase induction by β-lactamase inhibitors in *S. maltophilia* K279a.

S. maltophilia isolate K279a was incubated in presence of different potential inducers (cefoxitin, clavulanic acid, the bicyclic boronate **2**, or avibactam) at 50 $mg.L^{-1}$). L1 activity was measured from the cell extracts in a 96-well plate reader by determining meropenem hydrolysis (100 μM) at λ=300 nm. Protein concentration was determined by using the BioRad protein assay dye reagent. Specific activity was calculated by using the extinction coefficient of 9600 $AU.M^{-1}.cm^{-1}$ and a pathlength correction for the microplate (0.62 cm). Data presented are means +/- SEM, n=3.

Figure 4. L1 activity of inhibitor resistant mutants

In (A), L1 protein abundance data (relative to mean ribosomal protein abundance for each sample). Full proteomics data are shown in Tables S5 and S6. In (B), L1 enzyme activity in cell extracts is reported as meropenem hydrolysis rate. Data are reported as mean +/- SEM, n=3 for the parent strain, M11, and the two mutants (MB25 and MA27), which are resistant to ceftazidime/avibactam and ceftazidime/**2**.

Figure 5. Bicyclic boronate and avibactam binding conformations in Class A β-lactamases.

Superposition of inhibitors, shown as sticks, bound in the active sites of Class A β-lactamases. (A) Bicyclic boronates bound to L2 (blue, bicyclic boronate **2**) and CTX-M-15 (grey, bicyclic boronate **1**). (B) Avibactam bound to L2 (blue), SHV-1 (grey), KPC-2 (green) and CTX-M-15 (orange). Note the common binding mode for the bicyclic boronate bicyclic core and most of the avibactam structure; there are differences in the orientations of the avibactam core derived

SUPPLEMENTARY DATA FOR:

Structural/mechanistic insights into the efficacy of non-classical β-lactamase inhibitors against extensively drug resistant *Stenotrophomonas maltophilia* clinical isolates.

Karina Calvopiña[1], Philip Hinchliffe[1], Jürgen Brem[2], Samar Johnson[1], Kate J. Heesom[3], Ricky Cain[4], Christopher T. Lohans[2], Colin W. G. Fishwick[4], Christopher J. Schofield[2], James Spencer[1], Matthew B. Avison[1]*.

[1]School of Cellular & Molecular Medicine, University of Bristol, Bristol, United Kingdom.

[2]Department of Chemistry, University of Oxford, Oxford, United Kingdom.

[3]Bristol University Proteomics Facility, Bristol. United Kingdom.

[4]School of Chemistry, University of Leeds, Leeds. United Kingdom.

***Correspondence to: School of Cellular & Molecular Medicine, University of Bristol, Biomedical Sciences Building, University Walk. Bristol BS81TD, United Kingdom.**

bimba@bris.ac.uk.

Supplemental Figure 1. Efflux pump production in *S. maltophilia* mutants

Protein abundance data (relative to mean ribosomal protein Abundance for each sample) is reported as mean +/- Standard Error of the Mean (n=3). Full proteomics data are shown in Tables S1 and S2.

A

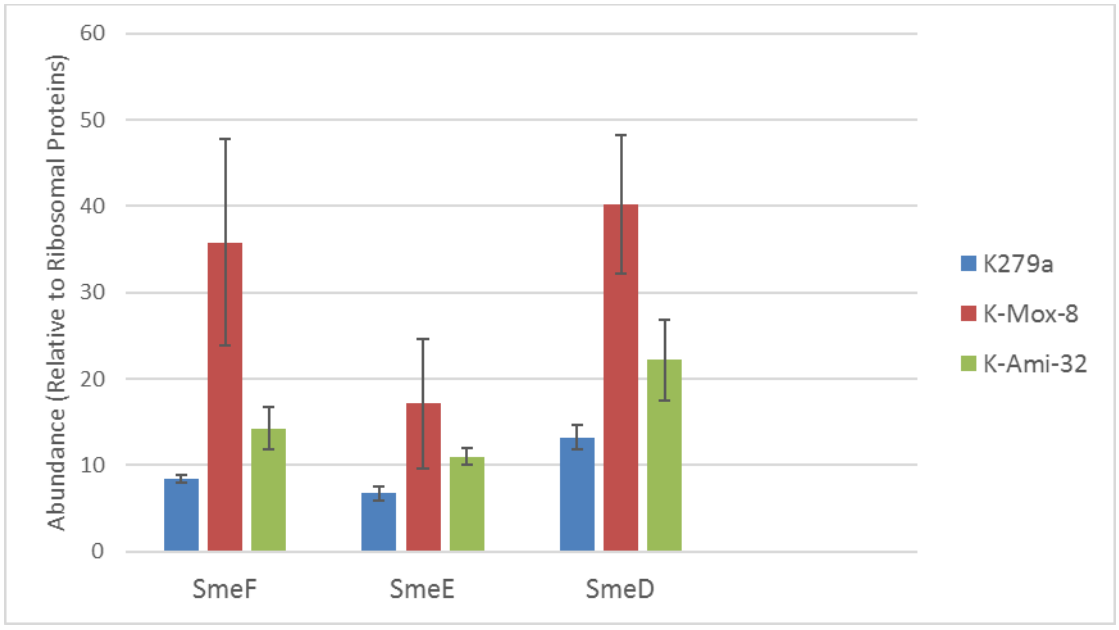

B

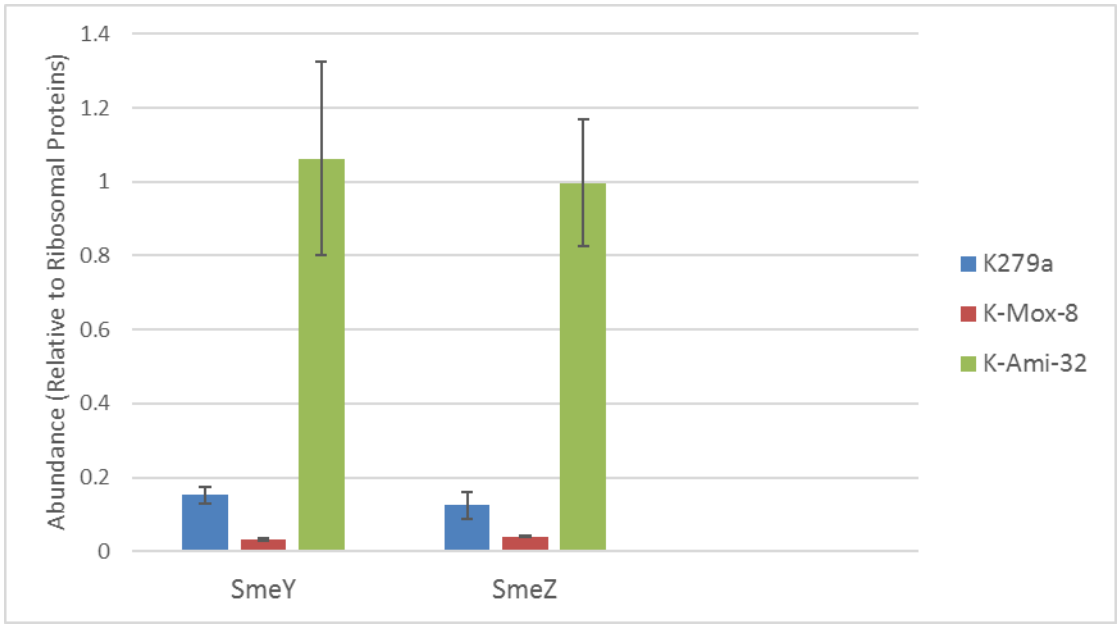

Supplemental Figure 2. Impact of Avibactam and Bicyclic Boronate 2 on Meropenem Hydrolysis by L1 as monitored by NMR spectroscopy. Impact of avibactam (75 μM) or bicyclic boronate **2** (75 μM) on the hydrolysis rate of meropenem (1 mM) as catalyzed by L1 (75 nM) in 50 mM Tris-d_{11}, pH 7.5, 10 % D_2O.

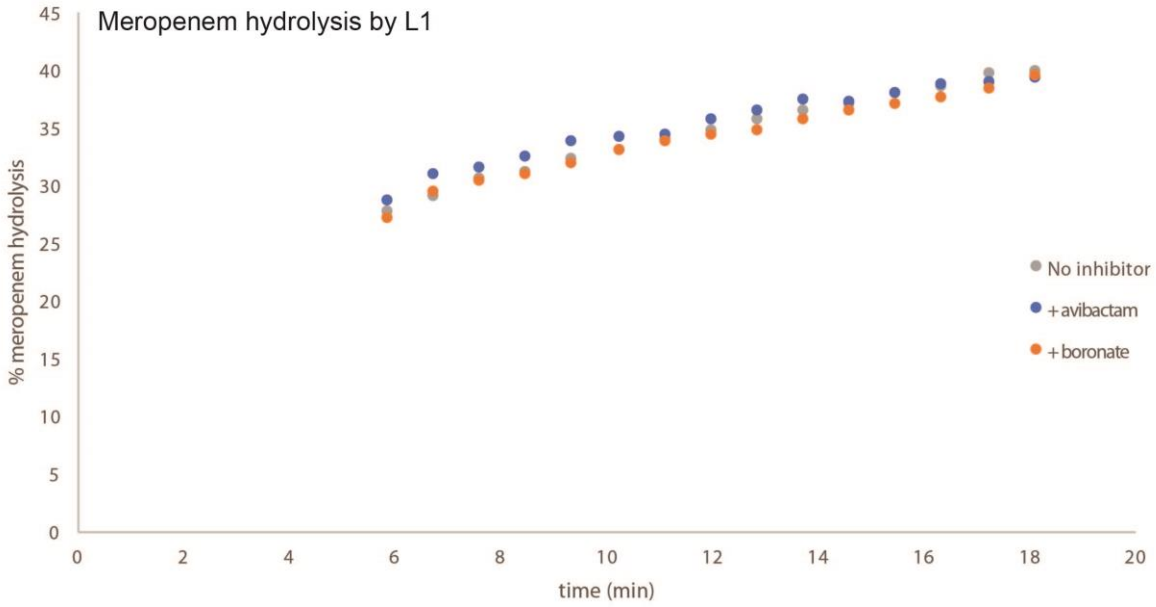

Supplemental Figure 3. Hydrolysis of Avibactam and Bicyclic Boronate 2 by L1 as monitored by NMR spectroscopy. (A) Hydrolysis of avibactam (400 μM) as catalysed by L1 (10 μM), in 50 mM Tris-d_{11}, pH 7.5, 10 % D_2O. Signals corresponding to hydrolysed avibactam are indicated with asterisks (*). (B) Incubation of bicyclic boronate **2** (400 μM) for 24 h with and without L1 (10 μM), all in 50 mM Tris-d_{11}, pH 7.5, 10 % D_2O.

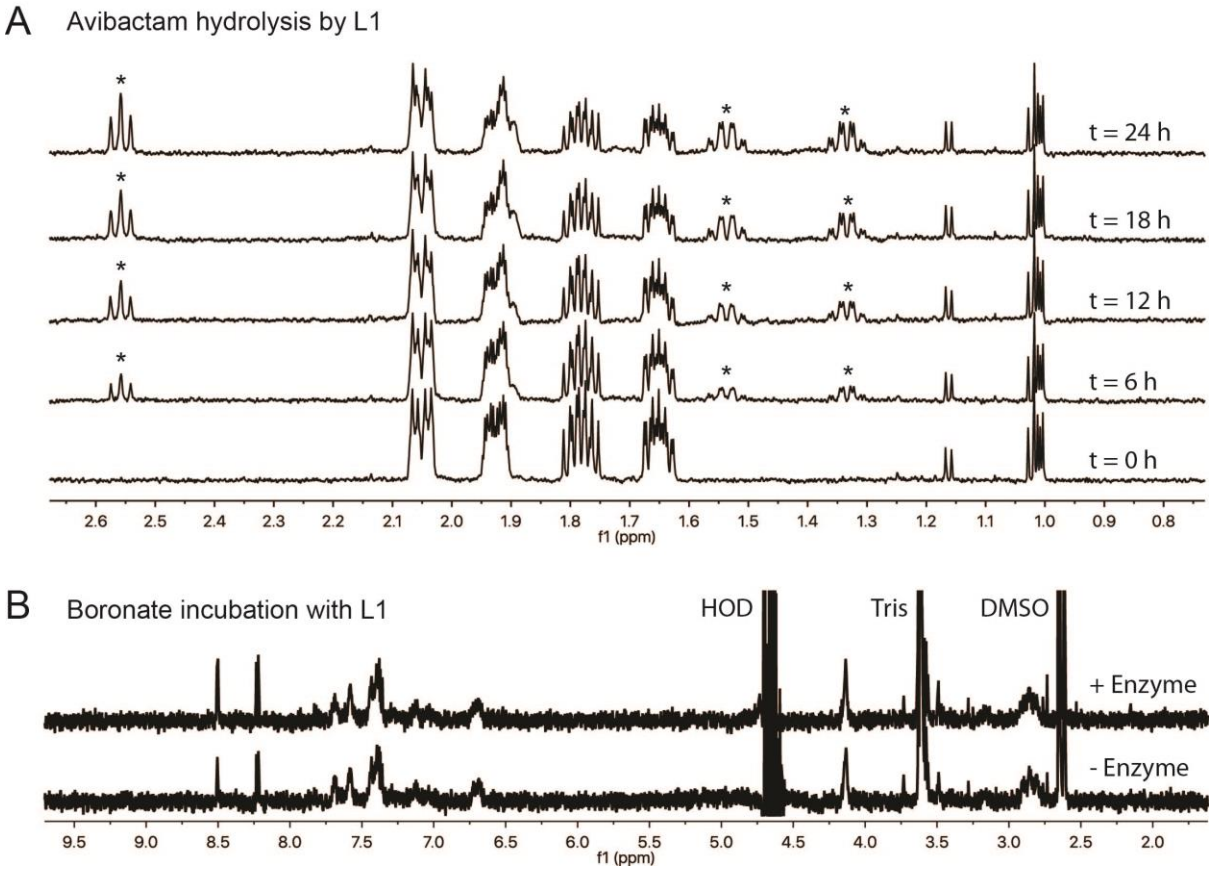

Supplemental Figure 4. L2 active site views showing electron density maps calculated after removal of ligand.

F_o-F_c density (green, contoured at 3σ) calculated from the final model after removal of (A) D-glutamate, (B) bicyclic boronate **2** and (C) avibactam. Residues coordinating the 'deacylating' water (red sphere, 'Wat') are shown as sticks and labelled (Ser70, Glu166 and Asn170).

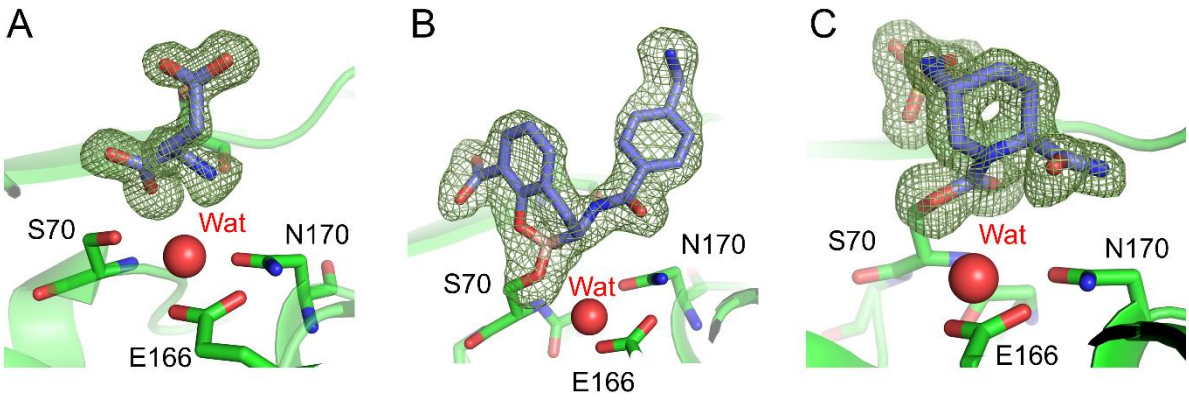

Supplemental figure 5. Comparison of the active sites of L2:D-glutamate with L2 native

L2:D-glutamate (green) and L2 native (PDB 1O7E, orange) are superposed and shown in cartoon, with important catalytic residues shown as sticks and the hydrolytic water (red) as a sphere.

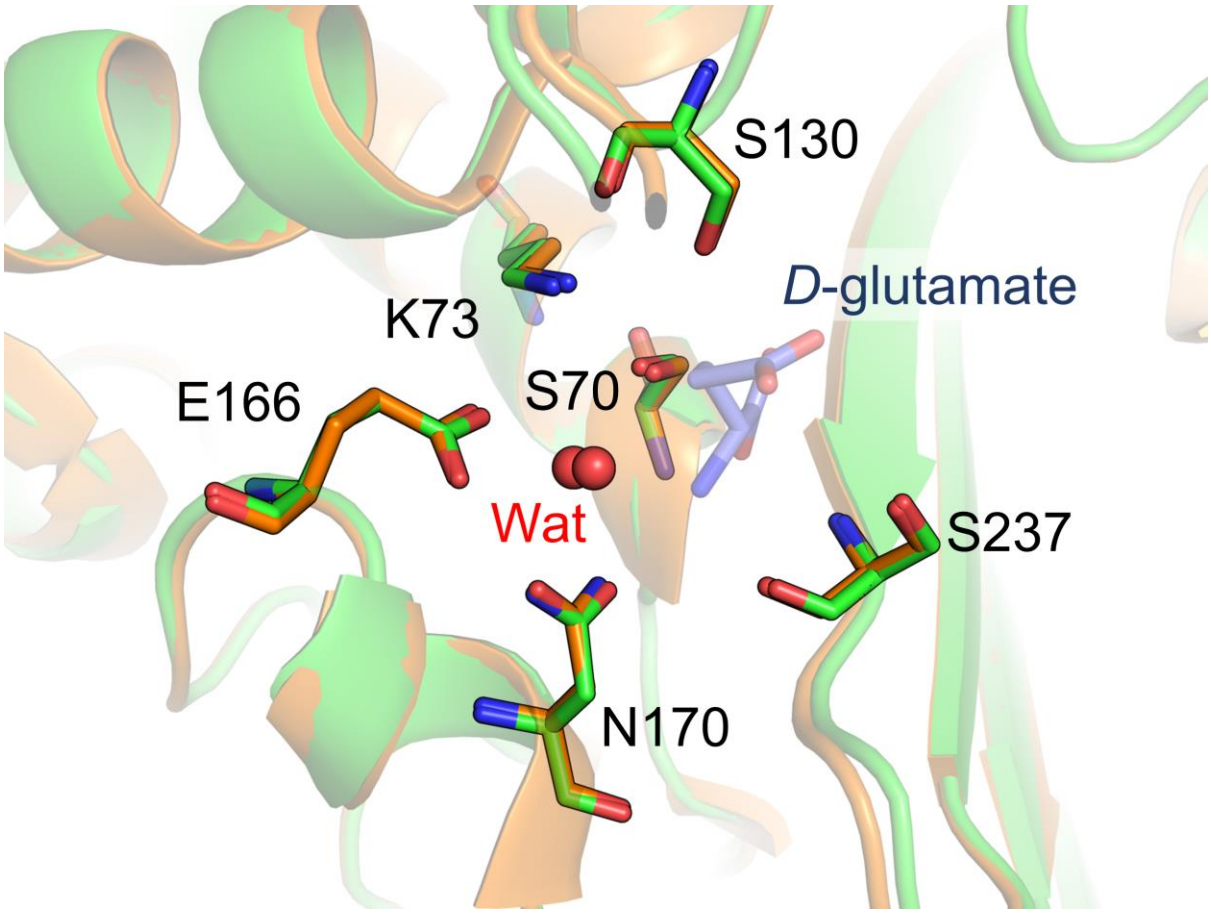

Supplemental Figure 6. Inhibitory effect of D-glutamate on L2 catalysis,

L2 activity reduces by 20% in presence of the highest concentration of D-glutamate (100 mM). Figure obtained by fitting residual activity plots using GraphPad Prism.

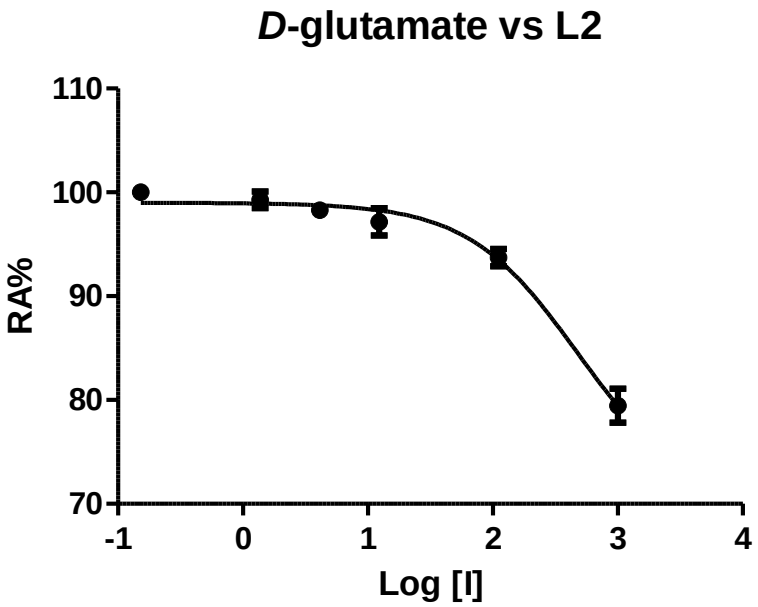

Supplemental Figure 7. Superposition of L2:D-glutamate with KPC-2:BLIP.

The L2:D-glutamate structure is superposed with the crystal structure (PDB 3E2K) of BLIP (yellow) bound in the active site of KPC-2 (grey). Asp49 (stick, labelled) is the only BLIP residue making interactions in the KPC-2 active site, although binding is significantly different to D-glutamate (blue), with the exception of hydrogen bond formation to the side chains of S130 and T237 (labelled sticks; S237 in L2). Residues which interact with the catalytic water (red sphere) or form the oxyanion hole are labelled and shown as sticks.

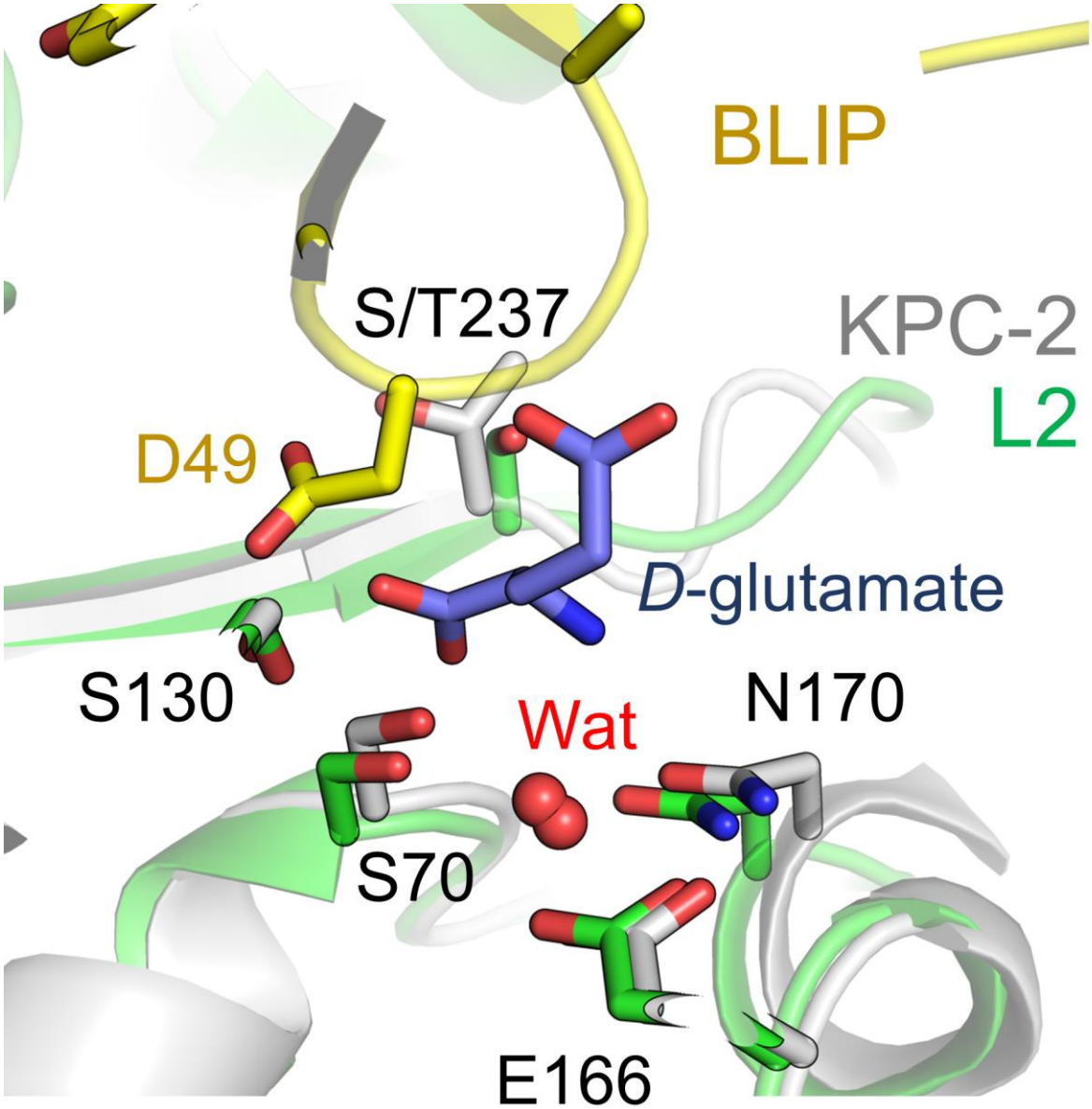

Supplemental Figure 8. Comparisons of structurally characterised modes of binding of avibactam in class A SBLs.

Avibactam (grey sticks) is shown as complexed with L2 (blue, this study), SHV-1 (orange, PDB 4ZAM), KPC-2 (green, PDB 4ZBE), and CTX-M-15 (cyan, PDB 4S2I).

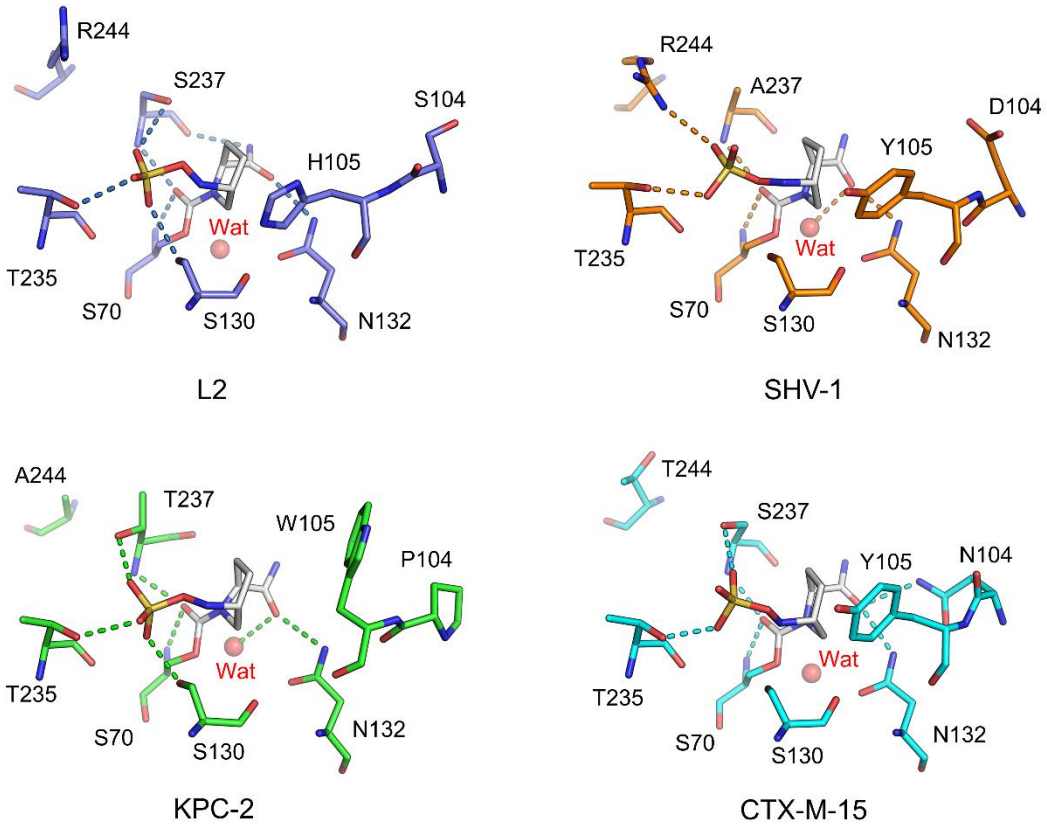

Supplemental Table 1

Normalised proteomics data for control and mutant K MOX 8 showing proteins whose abundance changes significantly according to a T-Test (P<0.05). Proteins that are >1.5 fold up and down regulated are highlighted green or red, respectively. Smaller changes are highlighted in orange.

K297a	K297a	K297a	K297a	K297a	K297a	KMOX8	KMOX8	KMOX8	Accession	T-Test (p=)	Fold
0.06	0.06	0.06	0.06	0.05		0.09	0.10		B2FNS0	0.000	1.65
0.30	0.42	0.39	0.47	0.39	0.36	0.19	0.16	0.19	B2FHJ2	0.000	0.46
10.55	14.85	14.80	16.30	11.27	11.45	47.38	24.22	48.95	B2FUV3	0.001	3.04
0.46	0.47	0.43	0.55	0.52	0.43	0.32	0.29	0.34	B2FNJ2	0.001	0.66
0.09	0.10	0.11	0.11	0.13	0.12	0.16	0.14	0.17	B2FUV6	0.002	1.43
5.87	5.81	5.80	6.24	4.94	5.54	3.88	3.58	4.89	B2FQN3	0.002	0.72
0.07	0.07	0.07	0.08	0.04	0.07	0.15	0.09	0.19	B2FMR3	0.003	2.16
0.26	0.33	0.31	0.32	0.43	0.23	0.12	0.12		B2FIF8	0.004	0.37
0.39	0.64	0.57	0.64	0.46	0.56	0.28	0.34	0.31	B2FHY7	0.004	0.57
0.18	0.11	0.18	0.18	0.12		0.04	0.03		B2FQ54	0.004	0.21
	0.03		0.03		0.03	0.05	0.05		B2FHI4	0.004	1.72
0.15	0.20	0.16	0.18	0.13	0.12	0.28	0.19	0.33	B2FJY1	0.004	1.75
0.09	0.04	0.06	0.07	0.06		0.13	0.12		B2FQQ5	0.004	1.99
31.82	26.81	24.65	21.36	24.84	32.41	16.83	14.13	19.97	B2FRM8	0.005	0.63
0.13	0.15	0.18	0.16	0.16	0.08	0.25	0.24	0.20	B2FLD2	0.005	1.57
0.12	0.13	0.11	0.12	0.09	0.11	0.13	0.13	0.15	B2FRD7	0.005	1.25
7.43	8.83	7.85	8.84	8.28	9.20	28.74	19.57	59.05	B2FUV1	0.005	4.26
2.07	2.50	1.94	2.19	1.76	2.16	3.20	2.48	3.97	B2FN03	0.005	1.53
0.11		0.12	0.14	0.10	0.08	0.17	0.22		B2FNQ5	0.005	1.79
0.25	0.40	0.42	0.43	0.29	0.43	0.55	0.49	0.63	B2FN87	0.005	1.50
0.07	0.12	0.10			0.11	0.03	0.04		B2FK89	0.006	0.34
2.55	3.69	2.75	2.80	2.81	2.01	5.00	3.33	6.07	B2FTY8	0.007	1.73
	0.07		0.08			0.05	0.05		B2FUK7	0.007	0.62
2.21	4.13	2.44	2.75	2.16	2.95	1.06	0.45	1.87	B2FR08	0.007	0.41
0.72	1.20	0.80	0.91	0.87	0.82	0.32	0.09	0.73	B2FP19	0.007	0.43
12.78	17.69	12.09	14.14	14.16	15.11	7.30	2.05	12.25	B2FJB1	0.008	0.50
1.69	2.22	1.73	2.08	2.12	1.78	3.56	2.39	5.58	B2FQG4	0.009	1.98
1.41	2.30	2.00	1.55	1.51	1.11	2.19	2.65	2.59	B2FHC7	0.010	1.50
0.29	0.42	0.36	0.37	0.27	0.31	0.51	0.46	0.88	B2FK09	0.010	1.83
1.63	2.15	1.63	2.10	1.79	1.37	1.04	0.83	1.51	B2FN47	0.011	0.63

0.23	0.38	0.30	0.32	0.38	0.43	0.47	0.74	1.37	B2FTA6	0.012	2.53
0.56	1.14	0.74	0.91	0.85	0.94	1.10	1.22	1.33	B2FUB3	0.012	1.42
0.83	0.09	0.38	0.47	0.40	0.39	1.25		0.81	B2FI10	0.013	2.42
0.63	0.85	0.68				0.94	0.94	1.00	B2FTU4	0.013	1.34
2.56	3.94	3.85	4.02	2.53	2.98	5.02	3.88	6.28	B2FNX6	0.013	1.53
0.77	0.85	0.98	0.97	0.71	0.95	1.25	0.94	1.53	B2FLV2	0.013	1.42
0.30	0.32	0.26	0.31	0.26	0.22	0.35	0.34	0.54	B2FLC2	0.013	1.48
0.13	0.21	0.17	0.18	0.12	0.12	0.22	0.22	0.36	B2FIS9	0.013	1.70
4.31	4.62	5.73	5.89	4.87	3.99	2.48	2.97	4.35	B2FRZ9	0.014	0.67
1.16	1.01	0.66	0.81	1.14	1.02	0.63	0.36	0.75	B2FLE4	0.014	0.60
0.14	0.16	0.13	0.14	0.24	0.23	0.27	0.27	0.55	B2FJ52	0.014	2.09
1.24	1.60	1.55	1.85	1.27	1.44	1.16	0.51		B2FNQ9	0.014	0.56
0.29	0.34	0.29	0.31	0.28	0.20	0.41	0.36	0.71	B2FUT9	0.014	1.73
0.27	0.35	0.30	0.33	0.27	0.30	0.29	0.20	0.19	B2FNK0	0.015	0.74
0.07	0.05	0.07	0.07	0.05	0.10	0.10	0.09	0.17	B2FQR3	0.016	1.73
0.38	0.47	0.46	0.37	0.33	0.28	0.59	0.50		B2FK79	0.017	1.43
0.18	0.33	0.26	0.31	0.25	0.23	0.37	0.31	0.39	B2FKN6	0.017	1.37
1.08	1.27	1.06	1.14	0.94	1.26	1.26	1.31	1.54	B2FSS7	0.018	1.22
1.72	2.02	1.82	1.98	1.49	1.95	1.54	1.10	1.62	B2FL10	0.018	0.78
2.85	3.70	2.73	2.95	2.90	2.88	4.63	3.64	8.78	B2FRM9	0.019	1.89
5.63	7.13	6.29	5.33	7.34	5.68	5.41	4.65	4.58	B2FHZ2	0.019	0.78
0.03		0.03				0.04	0.04		B2FU01	0.020	1.44
0.20	0.18	0.19	0.23	0.12	0.12	0.22	0.23	0.31	B2FJE9	0.020	1.45
4.57	5.84	5.51	6.18	3.92	3.95	3.77	3.32	3.44	B2FL08	0.020	0.70
0.64	0.55	0.99	1.04	0.70	1.02	0.33	0.31	0.69	B2FR42	0.021	0.54
0.58	0.40	0.69	0.64	0.40	0.53	0.35	0.40	0.30	B2FKJ7	0.021	0.65
0.62	0.69	0.65	0.78	0.61	0.65	0.28	0.38	0.69	B2FTM0	0.021	0.68
3.11	3.38	3.49	3.43	2.35	2.60	4.40	3.94	9.32	B2FUT2	0.023	1.92
0.04	0.06	0.04	0.05			0.13	0.15	0.06	B2FT83	0.023	2.30
0.55	0.77	0.55	0.65	0.52	0.49	0.91	0.80	2.15	B2FIJ2	0.023	2.18
0.15	0.17	0.17	0.18	0.13	0.17	0.20	0.24	0.52	B2FP51	0.024	1.97
0.42	0.71	0.59	0.67	0.49	0.75	0.27	0.20	0.58	B2FUR1	0.026	0.58
0.11	0.18	0.18	0.20	0.14	0.11	0.23	0.18	0.43	B2FMN4	0.026	1.85
1.02	1.06	0.75	0.79	0.92	0.62	0.79	0.43	0.51	B2FNL0	0.027	0.67
0.15	0.27	0.21	0.18	0.16	0.15	0.26	0.24	0.26	B2FTI8	0.027	1.36
0.06	0.05	0.04	0.04	0.05		0.09	0.05	0.10	B2FMR1	0.028	1.60

0.05	0.08	0.04	0.06			0.03	0.03		B2FN20	0.028	0.50
1.73	1.97	2.07	2.21	1.68	1.70	2.52	1.87	3.12	B2FUT4	0.029	1.32
0.39	0.40	0.36	0.42	0.23	0.52	0.49	0.46	0.69	B2FS15	0.030	1.43
0.05	0.07	0.10	0.04	0.05	0.10	0.13	0.10	0.36	B2FM97	0.030	2.77
	0.08	0.09	0.10	0.12		0.05	0.07		B2FNB1	0.030	0.61
1.58	1.38	1.03	1.10	0.99	1.43	1.14	0.84	0.58	B2FUB6	0.031	0.68
1.57	1.57	1.65	1.93	2.09	1.67	1.06	0.77	1.81	B2FHR9	0.031	0.70
		0.06	0.08	0.05		0.13	0.09	0.11	B2FLD3	0.032	1.61
0.34	0.34	0.26	0.36	0.24	0.27	0.41	0.34	0.79	B2FN23	0.032	1.69
0.25	0.46	0.34	0.48	0.16	0.40	0.18	0.15	0.23	B2FLT5	0.033	0.53
0.03	0.04	0.03			0.03	0.05	0.04	0.07	B2FKH5	0.033	1.60
1.68	2.15	1.74	1.82	1.08	1.75	1.93	2.13	3.19	B2FIJ0	0.034	1.42
0.11	0.13	0.12	0.13	0.10	0.07	0.16	0.14		B2FHZ8	0.035	1.33
0.02	0.07	0.13	0.07	0.04	0.23	0.30	0.08	0.49	B2FMC4	0.035	3.05
0.14	0.07		0.11			0.20		0.35	B2FUL3	0.036	2.59
3.89	5.96	3.92	4.75	3.81	8.45	7.09	6.39	11.74	B2FRS8	0.036	1.64
0.75	0.63	0.90	0.92	0.63	0.90	0.52	0.70	0.59	B2FJU4	0.036	0.76
1.44	1.79	1.22	1.42	0.85	1.57	1.93	1.45	2.77	B2FN30	0.036	1.48
2.50	2.45	1.76	2.12	2.01	2.42	2.89	2.69	7.13	B2FQG3	0.037	1.92
0.08	0.11	0.06	0.06	0.05	0.06	0.15	0.07	0.40	B2FJS8	0.037	3.02
0.20	0.32	0.24	0.26	0.25	0.31	0.16	0.04	0.27	B2FQ28	0.037	0.59
4.03	6.72	6.25	8.22	7.36	7.79	11.75	7.74	31.99	B2FUV2	0.038	2.55
0.16	0.22	0.19	0.23	0.15	0.21	0.17	0.33	0.59	B2FUS7	0.038	1.90
10.91	13.17	7.88	10.01	12.44	15.19	8.45	4.22	10.15	B2FP17	0.038	0.66
0.05	0.04	0.07	0.09	0.08	0.04	0.20	0.07		B2FT86	0.038	2.22
2.73	3.66	2.59	2.87	2.32	1.79	3.74	3.13	3.53	B2FQK4	0.039	1.30
0.08	0.18	0.15	0.16	0.14	0.05	0.05	0.07	0.07	B2FN57	0.039	0.50
1.27	1.61	1.93	1.95	1.09	1.79	2.35	1.97	6.43	B2FLV9	0.039	2.23
0.09	0.19	0.17	0.23	0.12	0.15	0.19	0.22	0.30	B2FMN7	0.040	1.49
0.56	0.62	0.58	0.66	0.37	0.55	0.68	0.66	1.58	B2FNN7	0.041	1.76
0.30	0.25	0.28	0.31	0.20	0.28	0.28	0.33	0.53	B2FUD9	0.041	1.41
1.33	1.22	1.15	1.20	1.13	0.81	0.77	1.09	0.80	B2FQ45	0.041	0.78
0.28	0.34	0.23	0.24	0.22	0.24	0.35	0.26	0.61	B2FSF4	0.042	1.57
0.15	0.13	0.19	0.22	0.15	0.16	0.11	0.10	0.15	B2FPD2	0.042	0.74
0.07	0.10	0.07	0.09	0.07	0.06	0.11	0.08	0.22	B2FJR1	0.042	1.75
1.25	1.71	1.24	1.35	1.53	0.98	1.80	1.36	2.97	B2FHG9	0.042	1.52

0.97	1.50	1.08	1.32	0.96	1.05	1.52	1.15	2.02	B2FN93	0.043	1.36
0.08		0.19	0.23	0.11	0.09	0.17	0.26	0.29	B2FSI7	0.043	1.71
	0.40	0.49			0.04	0.75	0.75		B2FQR8	0.044	2.43
0.06		0.05	0.05	0.06		0.13	0.07		B2FSF6	0.044	1.77
0.13	0.11	0.09	0.09	0.05	0.22	0.23	0.11	0.49	B2FQ71	0.044	2.40
0.31	0.37	0.32	0.27	0.32	0.29	0.34	0.34	0.56	B2FHD1	0.044	1.32
0.15	0.19	0.14	0.17	0.11	0.13	0.20	0.15	0.40	B2FSG4	0.045	1.71
0.06	0.08	0.09	0.08		0.08	0.06	0.06		B2FHE0	0.045	0.75
		0.05	0.05	0.05		0.04	0.04		B2FHZ7	0.047	0.81
0.10	0.15	0.16	0.20	0.10	0.15	0.21	0.18	0.67	B2FTS7	0.047	2.43
0.18	0.22	0.26	0.30	0.14	0.27	0.25	0.32	0.75	B2FMI1	0.048	1.92
0.24	0.31	0.26	0.24	0.20	0.29	0.27	0.30	0.57	B2FQ10	0.048	1.50
0.06	0.08	0.09	0.08	0.06	0.06	0.05	0.04	0.06	B2FNS9	0.048	0.74
0.50	0.66	0.55	0.60	0.35	0.25	0.30	0.21		B2FML3	0.049	0.52

Supplemental Table 2

Normalised proteomics data for control and mutant K AMI 32 showing proteins whose abundance changes significantly according to a T-Test (P<0.05). Proteins that are >1.5 fold up and down regulated are highlighted green or red, respectively. Smaller changes are highlighted in orange.

K297a	K297a	K297a	K297a	K297a	K297a	Kami32	Kami32	Kami32		Accession	T-Test (p=)	Fold
5.87	5.81	5.80	6.24	4.94	5.54	2.73	2.41		2.63	B2FQN3	0.000	0.45
0.04	0.10	0.11	0.16	0.10	0.23	0.86	0.79		1.34	B2FQ55	0.000	8.02
4.23	3.74	1.91	2.29	3.56	5.00	8.04	9.03		9.52	B2FQ35	0.000	2.57
0.04	0.05	0.04	0.04	0.04	0.02	0.07	0.08		0.08	B2FLG2	0.000	1.94
0.05	0.04	0.04	0.07	0.03		0.20	0.19		0.31	B2FTK1	0.000	5.01
0.56	0.71	0.68	0.55	0.58	0.80	1.06	1.03		0.90	B2FQ57	0.001	1.55
0.29	0.42	0.36	0.37	0.27	0.31	0.61	0.55		0.48	B2FK09	0.001	1.61
1.80	1.85	1.56	1.68	1.62	2.40	1.06	0.78		1.00	B2FND7	0.001	0.52
0.18	0.11	0.18	0.18	0.12		0.99	0.65		1.55	B2FQ54	0.002	7.01
0.04		0.06	0.06		0.07	0.12	0.10		0.16	B2FUF3	0.003	2.25
4.03	6.72	6.25	8.22	7.36	7.79	11.74	9.05		12.07	B2FUV2	0.003	1.63
0.76	0.97	0.72	0.75	0.83	1.18	0.56	0.44		0.30	B2FPY0	0.004	0.50
7.43	8.83	7.85	8.84	8.28	9.20	13.30	10.49		18.99	B2FUV1	0.005	1.70
0.07	0.07	0.08			0.08	0.43	0.20		0.26	B2FK32	0.006	3.88
0.12	0.13	0.11	0.12	0.09	0.11	0.09	0.06		0.08	B2FRD7	0.006	0.71
0.72	1.20	0.80	0.91	0.87	0.82	0.63	0.39		0.59	B2FP19	0.008	0.61
0.71	0.96	0.76	1.00	0.74	1.19	0.48	0.58		0.54	B2FMI9	0.009	0.60
1.07	1.14	0.89	0.89	0.91	1.01	0.75	0.71		0.86	B2FQ46	0.009	0.78
0.14		0.15	0.15		0.18	0.10	0.10			B2FKM5	0.009	0.64
1.58	1.38	1.03	1.10	0.99	1.43	0.71	0.92		0.75	B2FUB6	0.009	0.63
1.69	2.22	1.73	2.08	2.12	1.78	2.54	2.30		3.52	B2FQG4	0.010	1.44
0.15	0.19	0.14	0.17	0.11	0.13	0.22	0.20		0.19	B2FSG4	0.010	1.36
0.27	0.26	0.27	0.29	0.24	0.26	0.22	0.20		0.25	B2FMR0	0.010	0.84
0.56	1.14	0.74	0.91	0.85	0.94	0.38	0.64		0.39	B2FUB3	0.010	0.55
1.02	1.06	0.75	0.79	0.92	0.62	0.67	0.38		0.52	B2FNL0	0.010	0.61
4.57	5.84	5.51	6.18	3.92	3.95	2.84	3.35		3.48	B2FL08	0.011	0.65
1.63	1.57	1.56	1.53	1.37	1.85	1.36	1.37		0.96	B2FQ32	0.014	0.78
0.23	0.38	0.30	0.32	0.38	0.43	0.19	0.23		0.24	B2FTA6	0.014	0.65
0.24	0.29	0.24	0.15	0.21	0.28	0.13	0.19		0.11	B2FQ50	0.015	0.61

0.09	0.11	0.13	0.17	0.10	0.10	0.17	0.15	0.20	B2FNY3	0.015	1.46
0.72	0.70	0.57	0.69	0.49	0.73	0.41	0.52	0.52	B2FQJ6	0.016	0.74
0.64	0.76	0.65	0.72	0.57	0.59	0.61	0.46	0.43	B2FIR9	0.017	0.77
10.55	14.85	14.80	16.30	11.27	11.45	19.53	15.62	31.32	B2FUV3	0.017	1.68
0.98	1.14	0.82	0.75	1.24	1.05	0.86	0.59	0.55	B2FIN7	0.018	0.67
		0.02	0.03			0.04	0.04		B2FJE8	0.018	1.60
0.06	0.06	0.06	0.06	0.05		0.08	0.08	0.15	B2FNS0	0.019	1.84
0.27	0.15	0.19	0.18	0.12	0.20	0.36	1.08	0.33	B2FLW2	0.021	3.19
0.15	0.20	0.16	0.18	0.13	0.12	0.22	0.17	0.21	B2FJY1	0.023	1.31
31.82	26.81	24.65	21.36	24.84	32.41	23.07	17.50	20.46	B2FRM8	0.025	0.75
0.08		0.03	0.05	0.05	0.07	0.09	0.09	0.07	B2FME4	0.025	1.55
0.07	0.12	0.10			0.11	0.07	0.05		B2FK89	0.026	0.57
0.74	0.65	0.67	0.73	0.61	1.05	0.56	0.43	0.54	B2FT31	0.026	0.69
0.16	0.22	0.19	0.23	0.15	0.21	0.20	0.39	0.28	B2FUS7	0.027	1.50
5.58	5.03	4.34	4.55	5.16	5.89	4.20	4.63	3.75	B2FHC6	0.027	0.82
0.53	0.66	0.58	0.63	0.65	0.74	0.44	0.64	0.30	B2FPF2	0.029	0.72
0.08	0.11	0.06	0.06	0.05	0.06	0.13	0.06	0.17	B2FJS8	0.029	1.78
1.23	0.93	0.90	1.02	1.08	1.21	0.65	1.06	0.67	B2FTD2	0.030	0.75
0.03	0.07	0.06	0.07		0.05	0.08	0.07	0.09	B2FHT0	0.031	1.49
3.61	4.79	3.29	3.36	2.40	4.29	2.58	2.72	2.17	B2FIA9	0.031	0.69
0.04	0.05	0.04			0.04	0.06	0.05		B2FU50	0.031	1.31
1.58	1.57	0.99	1.08	1.06	1.34	0.77	1.16	0.69	B2FQJ4	0.035	0.69
0.06	0.08	0.05	0.06		0.07	0.05	0.04		B2FLC5	0.036	0.71
	0.09				0.08	0.07		0.06	B2FMN0	0.039	0.77
0.11	0.13	0.12	0.13	0.10	0.07	0.13	0.14	0.14	B2FHZ8	0.040	1.24
0.53	0.56	0.57	0.53	0.46	0.80	0.27	0.58	0.29	B2FQK1	0.040	0.66
2.21	4.13	2.44	2.75	2.16	2.95	2.20	1.16	2.00	B2FR08	0.041	0.64
1.38	1.36	1.15	1.35	1.17	1.49	1.23	1.16	1.02	B2FPR6	0.041	0.86
		0.06	0.08	0.05			0.11	0.09	B2FLD3	0.042	1.52
0.11	0.10	0.10		0.06	0.08	0.12	0.11	0.13	B2FNP1	0.044	1.31
0.38	0.45	0.35	0.39	0.35	0.89	0.28	0.22	0.16	B2FJH6	0.046	0.47
0.50	0.66	0.55	0.60	0.35	0.25	0.28	0.28	0.35	B2FML3	0.047	0.62
0.20	0.31	0.22	0.29	0.18	0.22	0.36	0.28	0.28	B2FT45	0.048	1.28
0.09		0.06	0.11		0.13	0.06	0.05	0.07	B2FK13	0.048	0.64
0.18	0.08	0.05	0.06	0.09	0.03	0.49	0.19	0.07	B2FS41	0.049	3.09
0.16	0.33	0.24	0.27	0.19	0.47	0.14	0.16	0.15	B2FSH7	0.049	0.54

Supplemental Table 3. Data collection and refinement statistics

	Native/D-glutamate	avibactam	bicyclic boronate **2**
Data collection			
Space group	$P2_12_12$	$P2_12_12$	$P2_12_12$
Molecules/ASU	2	2	2
Cell dimensions			
a, *b*, *c* (Å)	69.68, 84.72, 93.71	69.49, 84.31, 93.67	70.38, 85.69, 113.18
α, β, γ (°)	90.0, 90.0, 90.0	90.0, 90.0, 90.0	90.0, 90.0, 90.0
Wavelength(s) (Å)	0.97625	0.97949	0.92819
Resolution (Å)*	55.92 – 1.19 (1.21 – 1.19)	53.62 – 1.35 (1.37 – 1.35)	44.10 – 2.09 (2.14 – 2.09)
R_{pim}	0.050 (0.778)	0.053 (0.806)	0.126 (0.800)
$CC_{1/2}$	0.999 (0.625)	0.998 (0.616)	0.992 (0.534)
$I / \sigma(I)$	10.7 (1.9)	9.8 (1.3)	8.0 (1.4)
Completeness (%)	99.7 (98.3)	96.8 (94.2)	99.3 (99.5)
Redundancy	8.6 (8.0)	11.5 (9.9)	13.1 (13.3)
Refinement			
Resolution (Å)	55.92 – 1.19	53.62 – 1.35	42.845 – 2.09
No. reflections	176,092	116,868	40,861
R_{work} / R_{free}	0.1522 / 0.1640	0.1618 / 0.1781	0.1756 / 0.2143
No. atoms			
Protein	8180	3478	4035
Solvent	763	644	335
Ligand	34	56	25
B-factors (Å^2)			
Protein	15.9	17.3	28.8
Solvent	29.3	34.5	41.2
Ligand	24.3[1]	22.45[2]	29.9[3]
R.m.s. deviations			
Bond lengths (Å)	0.007	0.011	0.010
Bond angles (°)	0.963	1.349	1.249
Ramachandran (%)			
Outliers	0.00	0.00	0.00
Favoured	97.38	97.36	97.16

*Values in parentheses are for highest-resolution shell.
[1]Chain A B-factor 18.4; chain B B-factor 30.3
[2]Chain A B-factor 22.9; chain B B-factor 22.0
[3]Only present in chain B.

Supplemental Table 4. Catalytic water interactions (distances in Å) in L2 structures.

	Glu166-OE2	**Asn170-OD1**	**Ser70-OG**
L2:native (PDB 1O7E)	2.50	2.71	2.71
L2:D-glutamate	2.63	2.63	2.55
L2:avibactam	2.55	2.76	2.87
L2:bicyclic boronate 2	2.49	2.60	2.70

Supplemental Table 5

Protein abundance data (normalised using the mean average ribosomal protein) is provided for parent strain (M11) and mutant MA27 showing only proteins whose abundance changes significantly according to a T-Test (P<0.05) in the mutant relative to the parent strain. Proteins that are >1.5 fold up and down regulated are highlighted green or red, respectively. Smaller changes are highlighted in orange.

Accession	M11	M11	M11	MA27	MA27	MA27	T-Test (p=)	Fold
B2FHB7	0.04	0.09	0.05	0.22	0.19	0.20	0.001	3.35
B2FHC6	0.08	0.08	0.08	0.05	0.07	0.06	0.008	0.78
B2FHF0	0.11	0.27	0.29	0.66	0.44	0.40	0.024	2.22
B2FHG8	0.05	0.05	0.04	0.08	0.09	0.07	0.002	1.83
B2FHH6	0.03	0.10	0.11	0.19	0.17	0.12	0.029	2.07
B2FHH7	0.11	0.08	0.07	0.04	0.04	0.04	0.005	0.44
B2FHI0	0.07	0.04	0.05	0.10	0.08	0.07	0.044	1.53
B2FHI7	0.03	0.05	0.04	0.09	0.09	0.09	0.000	2.20
B2FHL9	0.01	0.02	0.02	0.01	0.01	0.01	0.043	0.68
B2FHR9	0.02	0.01	0.01	0.03	0.03	0.03	0.001	2.23
B2FHX0	0.03	0.04	0.03	0.07	0.06	0.06	0.004	1.63
B2FHX6	0.06	0.07	0.06	0.15	0.11	0.11	0.005	1.91
B2FHY8	0.21	0.19	0.47	1.37	0.88	1.23	0.004	4.01
B2FHZ0	0.49	0.57	0.60	1.33	0.92	1.24	0.005	2.10
B2FHZ1	0.06	0.03	0.04	0.13	0.09	0.08	0.018	2.32
B2FHZ7	0.22	0.28	0.20	0.40	0.30	0.32	0.025	1.45
B2FHZ8	0.24	0.25	0.27	0.33	0.26	0.31	0.041	1.18
B2FI00	0.09	0.08	0.23	0.33	0.31	0.24	0.021	2.20
B2FI56	0.01	0.02	0.02	0.02	0.03	0.03	0.029	1.78
B2FI93	0.12	0.10	0.13	0.20	0.20	0.13	0.041	1.50
B2FIA8	0.17	0.61	0.79	1.59	1.38	1.17	0.009	2.64
B2FID4	0.02	0.02	0.02	0.01	0.01	0.01	0.004	0.63
B2FIF8	0.07	0.18	0.29	0.40	0.35	0.32	0.030	1.96
B2FIH6	0.01	0.02	0.01	0.04	0.03	0.03	0.007	2.62
B2FIM3	0.27	0.26	0.17	0.10	0.19	0.08	0.034	0.52
B2FIQ4	0.02	0.02	0.03	0.02	0.02	0.02	0.026	0.71
B2FIT1	0.02	0.03	0.03	0.03	0.03	0.04	0.029	1.51
B2FJ17	0.05	0.10	0.08	0.14	0.12	0.12	0.020	1.66
B2FJ52	0.01	0.03	0.03	0.07	0.04	0.05	0.016	2.18
B2FJB1	0.43	0.29	0.22	0.13	0.14	0.12	0.019	0.40
B2FJE8	0.11	0.16	0.13	0.27	0.33	0.22	0.006	2.10
B2FJP9	0.04	0.06	0.07	0.11	0.09	0.11	0.010	1.79
B2FJQ0	0.02	0.05	0.04	0.07	0.07	0.07	0.006	1.97
B2FJQ8	0.16	0.14	0.14	0.11	0.09	0.09	0.003	0.65
B2FJR0	0.20	0.14	0.16	0.12	0.10	0.10	0.016	0.63
B2FJR8	0.44	0.40	0.30	0.68	0.57	0.50	0.019	1.53
B2FJS2	0.01	0.05	0.03	0.07	0.06	0.05	0.043	1.91
B2FJY2	0.01	0.01	0.01	0.02	0.03	0.02	0.001	2.33
B2FJY7	0.09	0.07	0.09	0.04	0.03	0.03	0.001	0.44
B2FK84	0.02	0.02	0.10	0.13	0.11	0.12	0.019	2.66
B2FK88	0.16	0.30	0.22	0.42	0.43	0.38	0.006	1.82
B2FK94	0.00	0.02	0.02	0.07	0.05	0.04	0.007	3.87

B2FKA2	0.02	0.02	0.02	0.02	0.02	0.02	0.042	0.86
B2FKE4	0.03	0.08	0.06	0.13	0.09	0.08	0.042	1.76
B2FKE8	0.01	0.01	0.01	0.04	0.04	0.04	0.000	4.42
B2FKH7	0.04	0.05	0.03	0.03	0.03	0.02	0.030	0.61
B2FKI7	0.02	0.05	0.04	0.07	0.07	0.05	0.039	1.58
B2FKK2	0.10	0.16	0.17	0.20	0.23	0.21	0.022	1.47
B2FKK6	0.01	0.02	0.03	0.04	0.04	0.04	0.019	2.01
B2FKK7	0.13	0.12	0.11	0.08	0.08	0.05	0.006	0.59
B2FKL5	0.01	0.01	0.01	0.03	0.03	0.03	0.001	2.52
B2FKM0	0.01	0.05	0.06	0.10	0.09	0.06	0.046	2.07
B2FKN8	0.02	0.04	0.04	0.08	0.10	0.06	0.011	2.56
B2FKN9	0.03	0.05	0.05	0.11	0.12	0.08	0.008	2.25
B2FKP1	0.01	0.03	0.05	0.06	0.05	0.05	0.044	1.93
B2FKR0	0.05	0.08	0.05	0.09	0.09	0.09	0.019	1.54
B2FKU5	0.02		0.01	0.06	0.05	0.03	0.039	3.27
B2FKU7	0.02	0.03	0.03	0.03	0.04	0.03	0.029	1.32
B2FKV6	0.01	0.01	0.02	0.07	0.05	0.05	0.002	4.31
B2FL08	0.13	0.12	0.13	0.05	0.03	0.04	0.000	0.30
B2FL10	0.03	0.04	0.05	0.03	0.01	0.01	0.045	0.43
B2FL31	0.13	0.14	0.19	0.13	0.09	0.09	0.044	0.67
B2FL33	0.14	0.11	0.10	0.15	0.14	0.14	0.035	1.28
B2FL58	0.00	0.01	0.01	0.02	0.02	0.02	0.006	2.03
B2FL60	0.02	0.02	0.02	0.03	0.03	0.02	0.007	1.31
B2FL62	0.18	0.13	0.12	0.10	0.09	0.10	0.035	0.68
B2FL71	0.02	0.06	0.04	0.08	0.08	0.07	0.011	1.94
B2FL86	0.20	0.17	0.19	0.14	0.11	0.13	0.003	0.66
B2FL97	0.01	0.03	0.03	0.05	0.04	0.05	0.011	2.04
B2FLB0	0.03	0.04	0.04	0.07	0.07	0.05	0.011	1.62
B2FLB7	0.02	0.02	0.03	0.07	0.08	0.03	0.037	2.25
B2FLB8	0.03	0.12	0.14	0.20	0.18	0.15	0.047	1.87
B2FLB9	0.01		0.01	0.01	0.01	0.02	0.005	1.72
B2FLC7	0.01	0.02	0.02	0.08	0.05	0.07	0.003	3.56
B2FLC8	0.07	0.11	0.11	0.17	0.16	0.17	0.005	1.67
B2FLD3	0.30	0.49	0.35	0.53	0.57	0.54	0.022	1.44
B2FLE4	0.01	0.02	0.02	0.08	0.06	0.06	0.002	4.28
B2FLE9	0.07	0.07	0.06		0.09	0.10	0.008	1.48
B2FLG0	0.04	0.07	0.07	0.18	0.14	0.12	0.005	2.49
B2FLG2	0.39	0.33	0.22	0.15	0.20	0.13	0.022	0.51
B2FLQ1	0.02	0.02	0.03	0.01	0.01	0.01	0.004	0.48
B2FLR0	0.04	0.05	0.08	0.13	0.12	0.10	0.005	1.98
B2FLR1	0.22	0.24	0.19	0.26	0.30	0.27	0.015	1.26
B2FLT7	0.17	0.19	0.18	0.10	0.08	0.09	0.000	0.50
B2FLT8	0.03	0.04	0.04	0.08	0.09	0.06	0.004	2.28
B2FLU6	0.08	0.16	0.09	0.25	0.18	0.16	0.046	1.74
B2FLU7	0.04	0.10	0.05	0.15	0.12	0.10	0.032	1.88
B2FLV9	0.03	0.03	0.04	0.03	0.02	0.03	0.034	0.71
B2FLW5	0.26	0.20	0.25	0.14	0.15	0.16	0.004	0.64
B2FLW7	0.01	0.02	0.03	0.05	0.05	0.04	0.008	2.33
B2FMA5	0.07	0.17	0.14	0.23	0.20	0.19	0.039	1.64
B2FMB1	0.04	0.07	0.06	0.10	0.09	0.07	0.026	1.61
B2FME5	0.02	0.03	0.02	0.05	0.04	0.04	0.007	1.86
B2FME8	0.03	0.06	0.05	0.21	0.17	0.16	0.001	3.79
B2FMF0	0.03	0.07	0.05	0.09	0.10	0.09	0.011	1.76
B2FMF5	0.01	0.02	0.01	0.04	0.03	0.03	0.025	1.93
B2FMF6	0.25		0.06	0.61	0.53	0.36	0.031	3.15
B2FMH2	0.02	0.03	0.03	0.05	0.04	0.04	0.007	1.63

B2FMI0	0.03	0.04	0.04	0.07	0.07	0.06	0.002	1.81
B2FMK4	0.01	0.04	0.03	0.06	0.05	0.04	0.033	1.84
B2FML2	0.05		0.04	0.03	0.03	0.02	0.017	0.59
B2FMP5	0.08	0.15	0.19	0.32	0.22	0.21	0.043	1.78
B2FMP6	0.05	0.08	0.12	0.22	0.14	0.16	0.024	2.06
B2FMP7	0.05	0.06	0.09	0.15	0.16	0.13	0.002	2.25
B2FMP8	0.03	0.09	0.09	0.16	0.15	0.11	0.021	2.07
B2FMP9	0.03	0.08	0.08	0.15	0.13	0.11	0.018	1.95
B2FMQ2	0.00	0.02	0.02	0.04	0.03	0.03	0.015	2.34
B2FMR5	0.09	0.13	0.10	0.14	0.15	0.14	0.029	1.34
B2FMS4	0.22	0.40	0.28	0.46	0.40	0.53	0.035	1.54
B2FMT2	0.03	0.04	0.03	0.08	0.06	0.05	0.021	1.69
B2FMX9	0.05	0.02	0.03	0.07	0.07	0.08	0.014	2.18
B2FMY5	1.04	1.00	1.05	1.51	1.60	1.20	0.015	1.39
B2FMY6	0.06	0.07	0.12	0.19	0.15	0.15	0.010	1.96
B2FMZ8	0.03	0.07	0.05	0.10	0.11	0.09	0.009	2.15
B2FN02	0.06	0.06	0.06	0.05	0.04	0.05	0.017	0.75
B2FN04	0.14	0.30	0.19	0.36	0.32	0.29	0.049	1.53
B2FN25	0.02	0.08	0.07	0.14	0.13	0.08	0.048	1.99
B2FN26	0.01	0.03	0.03	0.06	0.04	0.03	0.041	1.98
B2FN45	0.03	0.05	0.04	0.06	0.05	0.04	0.048	1.44
B2FN47	0.05	0.04	0.02	0.01	0.01	0.01	0.014	0.26
B2FN55	0.04	0.06	0.03	0.09	0.08	0.08	0.005	1.85
B2FN74	0.14	0.10	0.12	0.09	0.08	0.09	0.029	0.72
B2FN91	0.06	0.13	0.15	0.34	0.26	0.31	0.002	2.65
B2FN93	0.03	0.04	0.05		0.02	0.02	0.032	0.53
B2FNA0	0.00	0.01		0.02	0.02	0.02	0.010	2.71
B2FND9	0.05	0.03	0.04	0.03	0.01	0.02	0.025	0.50
B2FNF2	0.02	0.06	0.06	0.01	0.01	0.01	0.027	0.22
B2FNG6	0.06	0.09	0.06	0.14	0.14	0.12	0.001	1.90
B2FNJ3	0.01	0.03	0.03	0.07	0.05	0.04	0.017	2.26
B2FNK2	0.07	0.21	0.15	0.32	0.30	0.30	0.009	2.13
B2FNL4	0.14	0.10	0.11	0.09	0.09	0.09	0.043	0.76
B2FNN8	0.02	0.05	0.07	0.08	0.08	0.08	0.031	1.84
B2FNN9	0.01	0.02	0.02	0.06	0.05	0.04	0.003	3.36
B2FNQ2	0.02	0.08	0.06	0.12	0.14	0.09	0.028	2.10
B2FNQ3	0.08	0.07	0.05	0.11	0.11	0.09	0.022	1.53
B2FNS1	0.06	0.09	0.08	0.24	0.14	0.17	0.012	2.49
B2FNX1	0.08	0.05	0.06	0.03		0.02	0.020	0.37
B2FNX3	0.09	0.16	0.18	0.24	0.22	0.22	0.015	1.63
B2FNY1	0.01	0.06	0.09	0.13	0.13	0.12	0.011	2.46
B2FNZ9	0.01	0.02	0.03	0.23	0.17	0.18	0.001	8.57
B2FP02	0.02	0.08	0.07	0.11	0.11	0.09	0.040	1.84
B2FP05	0.02	0.02		0.02	0.02		0.038	1.21
B2FP16	0.84	0.65	0.43	0.34	0.34	0.30	0.029	0.51
B2FP17	0.50	0.37	0.27	0.13	0.22	0.19	0.025	0.48
B2FP29	0.05		0.02	0.18	0.11	0.15	0.014	4.22
B2FP47	0.08	0.11	0.10	0.14	0.13	0.14	0.006	1.43
B2FP69	0.01	0.01	0.01	0.04	0.03	0.02	0.013	2.43
B2FP70	0.01	0.01	0.06	0.08	0.07	0.07	0.024	2.69
B2FP85	0.03	0.15	0.13	0.21	0.21	0.16	0.042	1.89
B2FP88	0.02	0.05	0.03	0.05	0.07	0.04	0.046	1.62
B2FPA5	0.05	0.06	0.07	0.05	0.03	0.04	0.026	0.68
B2FPC4	0.04	0.05	0.03	0.03	0.03	0.03	0.036	0.69
B2FPC7	0.16	0.31	0.17	0.51	0.37	0.39	0.016	1.96
B2FPD8	0.03	0.14	0.13	0.25	0.20	0.18	0.026	2.15

B2FPE4	0.04		0.01	0.54	0.43	0.39	0.002	19.68
B2FPH2	0.01	0.01	0.01	0.01	0.01	0.01	0.025	0.70
B2FPH9	0.07	0.11	0.09	0.15	0.16	0.14	0.005	1.75
B2FPI7	0.01	0.01	0.01	0.02	0.02	0.02	0.030	1.69
B2FPJ1	0.05	0.07	0.07	0.19	0.15	0.15	0.001	2.61
B2FPL6	0.02	0.04	0.04	0.09	0.07	0.08	0.004	2.20
B2FPN5	0.03	0.03	0.02	0.01	0.01	0.01	0.003	0.27
B2FPQ0	0.01	0.01	0.01	0.05	0.03	0.04	0.003	3.78
B2FPQ1	0.01	0.01	0.01	0.03	0.03	0.02	0.001	3.37
B2FPT0	0.08	0.06	0.07	0.11	0.09	0.09	0.028	1.36
B2FPV8	0.04	0.03	0.05	0.05	0.05	0.05	0.016	1.30
B2FPW8	0.06	0.18	0.13	0.28	0.22	0.20	0.027	1.92
B2FPY6	0.01	0.04	0.02	0.09	0.04	0.06	0.032	2.45
B2FQ05	0.06	0.12	0.11	0.24	0.21	0.17	0.009	2.12
B2FQ07	0.03	0.03	0.03	0.04	0.04	0.04	0.002	1.21
B2FQ14	0.00	0.01	0.01	0.01	0.01	0.01	0.030	2.12
B2FQ19	0.01	0.04	0.04	0.09	0.07	0.05	0.023	2.27
B2FQ34	1.65	1.16	1.40	0.96	0.91	1.18	0.039	0.73
B2FQ36	0.15	0.19	0.25	0.58	0.35	0.57	0.009	2.56
B2FQ38	0.57	0.41	0.50	0.37	0.29	0.37	0.023	0.69
B2FQ52	1.43	0.94	1.02	0.70	0.68	0.88	0.042	0.67
B2FQ58	0.02	0.05	0.06	0.14	0.11	0.10	0.007	2.78
B2FQ70	0.01	0.02	0.02	0.04	0.03	0.02	0.039	1.87
B2FQ71	0.03	0.04	0.05	0.10	0.08	0.09	0.002	2.33
B2FQ72	0.08	0.10	0.10	0.20	0.17	0.18	0.001	1.88
B2FQ82	0.00	0.01	0.00	0.01	0.01	0.01	0.005	2.64
B2FQ88	0.01	0.01	0.01	0.01	0.01	0.00	0.010	0.64
B2FQ90	0.02	0.03	0.03	0.07	0.07	0.08	0.000	3.02
B2FQC5	0.03	0.06	0.07	0.13	0.11	0.11	0.005	2.14
B2FQE3	0.08	0.07	0.07	0.05	0.04	0.04	0.005	0.63
B2FQG0	0.02	0.05	0.12	0.14	0.15	0.12	0.043	2.03
B2FQJ5	0.31	0.17	0.26	0.45	0.54	0.64	0.006	2.22
B2FQJ8	1.82	1.30	1.24	0.79	0.97	1.08	0.034	0.65
B2FQL7	0.58	0.57	0.45	0.62	0.68	0.74	0.023	1.28
B2FQM3	0.02	0.04	0.04	0.09	0.09	0.07	0.006	2.58
B2FQN2	0.04	0.09	0.08	0.13	0.14	0.11	0.020	1.84
B2FQR1	0.10	0.19	0.21	0.42	0.28	0.35	0.012	2.11
B2FQR2	0.03	0.13	0.17	0.20	0.22	0.20	0.044	1.85
B2FQR3	0.04	0.05	0.07	0.10	0.07	0.09	0.035	1.54
B2FQU5	0.04	0.09	0.10	0.23	0.40	0.21	0.016	3.70
B2FQU6	0.03	0.07	0.10	0.22	0.39	0.20	0.017	4.03
B2FQU7	0.04	0.07	0.09	0.23	0.36	0.20	0.010	3.92
B2FQX4	0.02	0.02	0.03	0.10	0.09	0.11	0.000	4.93
B2FQY3	0.04	0.16	0.15	0.33	0.26	0.18	0.038	2.16
B2FQY5	0.06	0.07	0.06	0.11	0.11	0.11	0.000	1.71
B2FQZ2	0.01	0.02	0.02	0.03	0.02	0.02	0.042	1.55
B2FR08	0.06	0.05	0.03	0.03	0.03	0.02	0.041	0.64
B2FR21	0.07	0.11	0.09	0.16	0.20	0.13	0.012	1.89
B2FR38	0.01	0.02	0.02	0.05	0.04	0.03	0.013	2.80
B2FR50	0.09	0.22	0.24	0.39	0.28	0.32	0.030	1.79
B2FR55	0.04	0.07	0.08	0.10	0.08	0.10	0.033	1.52
B2FR86	0.01	0.01	0.07	0.09	0.07	0.06	0.044	2.48
B2FR89	0.05	0.10	0.13	0.18	0.14	0.15	0.032	1.71
B2FR91	0.11	0.25	0.21	0.38	0.29	0.27	0.044	1.62
B2FRF2	0.02	0.07	0.07	0.13	0.11	0.09	0.023	1.99
B2FRP1	0.07	0.20	0.13	0.27	0.24	0.24	0.023	1.87

B2FRP7	0.04	0.03	0.04	0.02	0.01	0.02	0.013	0.55
B2FRR1	0.02	0.02	0.01	0.04	0.04	0.05	0.001	2.72
B2FRS1	0.01	0.02	0.02	0.02	0.03	0.03	0.013	2.09
B2FRS2	0.14	0.23	0.31	0.50	0.40	0.46	0.007	2.00
B2FRS3	0.35	0.32	0.47	0.74	0.79	0.77	0.001	2.02
B2FRS8	0.55	0.34	0.60	0.09	0.14	0.23	0.010	0.31
B2FRT5	0.03	0.03	0.05	0.07	0.06	0.05	0.048	1.54
B2FRW3	0.11	0.07	0.10	0.15	0.17	0.19	0.004	1.87
B2FRW9	0.01	0.02	0.03	0.04	0.09	0.11	0.025	3.74
B2FRX1	0.06	0.10	0.08	0.12	0.12	0.09	0.036	1.42
B2FRZ2	0.02	0.10	0.09	0.36	0.28	0.19	0.010	3.93
B2FRZ3	0.02	0.03	0.02	0.11	0.11	0.10	0.000	4.38
B2FRZ9	0.07	0.05	0.04	0.19	0.17	0.19	0.000	3.51
B2FS02	0.01	0.02	0.02	0.04	0.03	0.03	0.002	1.99
B2FS05	0.02	0.02	0.02	0.04	0.03	0.03	0.006	1.90
B2FS08	0.01	0.03	0.03	0.05	0.04	0.05	0.038	1.69
B2FSE9	0.08	0.09	0.12	0.05	0.03	0.04	0.006	0.40
B2FSF0	0.12	0.38	0.37	0.66	0.55	0.44	0.033	1.90
B2FSF3	0.04	0.12	0.14	0.24	0.21	0.18	0.014	2.13
B2FSF6	0.04	0.14	0.20	0.32	0.24	0.34	0.021	2.31
B2FSF9	0.01	0.01	0.02	0.02	0.02	0.02	0.031	1.81
B2FSG5	0.26	0.31	0.22	0.39	0.38	0.35	0.009	1.42
B2FSI8	0.17	0.06	0.07	0.24	0.23	0.41	0.022	2.90
B2FST5	0.00	0.01	0.00	0.01	0.01	0.01	0.011	2.16
B2FSX8	0.01	0.02	0.02	0.03	0.03	0.04	0.030	1.95
B2FT04	0.01	0.01	0.01		0.00	0.00	0.042	0.36
B2FT38	0.04	0.08	0.07	0.10	0.11	0.09	0.014	1.69
B2FT49	0.01	0.03	0.02	0.04	0.05	0.04	0.005	2.13
B2FT66	0.18	0.15	0.12	0.10	0.11	0.09	0.037	0.67
B2FT86	0.11	0.31	0.25	0.50	0.47	0.34	0.025	1.97
B2FTA3	0.19	0.17	0.12	0.28	0.24	0.22	0.013	1.55
B2FTA7	0.05	0.08	0.09	0.17	0.11	0.13	0.021	1.92
B2FTD2	0.99	0.53	0.54	0.16	0.10	0.16	0.012	0.20
B2FTJ0	0.10	0.10	0.07	0.13	0.14	0.11	0.026	1.40
B2FTM1	0.06	0.15	0.20	0.55	0.54	0.34	0.006	3.53
B2FTR8	0.01	0.01	0.02	0.03	0.03	0.02	0.007	2.27
B2FTS4	0.05	0.07	0.11	0.16	0.13	0.15	0.013	1.87
B2FTV4	0.06	0.16	0.16	0.30	0.26	0.18	0.031	1.94
B2FTX1	0.02	0.06	0.06	0.10	0.09	0.07	0.029	1.81
B2FU11	0.15	0.38	0.26	0.46	0.44	0.36	0.047	1.61
B2FUA0	0.06	0.07	0.09	0.06	0.03	0.04	0.027	0.59
B2FUA1	0.08	0.06	0.08	0.06	0.04	0.06	0.018	0.72
B2FUA6	0.01	0.02	0.01	0.01		0.01	0.040	0.71
B2FUC5	0.01	0.01	0.02	0.01	0.00	0.01	0.024	0.43
B2FUE8	0.04	0.09	0.06	0.69	0.54	0.57	0.000	10.07
B2FUL2	0.06	0.06	0.06	0.02	0.03	0.01	0.001	0.32
B2FUR4	0.04		0.05	0.02	0.02	0.01	0.009	0.40
B2FUS7	0.03	0.03	0.03	0.05	0.06	0.06	0.004	1.83
B2FUU7	0.05	0.05	0.03	0.06	0.07	0.09	0.035	1.57
B2FUV3	0.07	0.14	0.16	0.22	0.17	0.19	0.044	1.56
B2FUV6	0.14	0.15	0.17	0.25	0.21	0.24	0.004	1.49

8

9

Supplemental Table 6

Protein abundance data (normalised using the mean average ribosomal protein) is provided for parent strain (M11) and mutant MB25 showing only proteins whose abundance changes significantly according to a T-Test (P<0.05) in the mutant relative to the parent strain. Proteins that are >1.5 fold up and down regulated are highlighted green or red, respectively. Smaller changes are highlighted in orange.

Accession	M11	M11	M11	MB25	MB25	MB25	T-Test (p=)	Fold
B2FHA2	0.01	0.01	0.01	0.01	0.01		0.048	0.66
B2FHA6	0.01	0.00		0.01	0.01	0.01	0.002	3.01
B2FHB7	0.04	0.09	0.05	0.19	0.18	0.17	0.001	3.00
B2FHF0	0.11	0.27	0.29	0.47	0.60	0.30	0.047	2.02
B2FHG8	0.05	0.05	0.04	0.07	0.06	0.06	0.003	1.47
B2FHH6	0.03	0.10	0.11	0.16	0.17	0.12	0.039	1.88
B2FHH7	0.11	0.08	0.07	0.04	0.05	0.03	0.007	0.46
B2FHH9	0.03	0.01	0.02	0.04	0.04	0.03	0.026	2.34
B2FHI0	0.07	0.04	0.05	0.09	0.10	0.06	0.036	1.56
B2FHI7	0.03	0.05	0.04	0.08	0.09	0.06	0.009	1.83
B2FHW7	0.01	0.02	0.02	0.04	0.04	0.03	0.010	2.28
B2FHX0	0.03	0.04	0.03	0.06	0.06	0.05	0.007	1.55
B2FHX6	0.06	0.07	0.06	0.12	0.10	0.09	0.010	1.59
B2FHY7	0.13	0.15	0.14	0.15	0.19	0.19	0.035	1.26
B2FHY8	0.21	0.19	0.47	0.69	0.48	0.96	0.032	2.44
B2FHZ0	0.49	0.57	0.60	0.93	0.71	1.27	0.032	1.75
B2FHZ7	0.22	0.28	0.20	0.35	0.34	0.26	0.044	1.35
B2FHZ8	0.24	0.25	0.27	0.34	0.34	0.27	0.034	1.24
B2FI55	0.02	0.03	0.02	0.05	0.05	0.05	0.000	2.46
B2FI56	0.01	0.02	0.02	0.04	0.03	0.04	0.009	2.26
B2FI57	0.02	0.04	0.03	0.06	0.06	0.05	0.005	1.86
B2FI80	0.03	0.03	0.03	0.06	0.07	0.05	0.001	1.99
B2FI81	0.01	0.01	0.01	0.03	0.02	0.02	0.015	2.06
B2FI82	0.01	0.03	0.02	0.07	0.09	0.06	0.005	3.83
B2FI93	0.12	0.10	0.13	0.22	0.20	0.15	0.015	1.64
B2FIA6	0.04	0.07	0.12	0.15	0.17	0.12	0.038	1.90
B2FIA8	0.17	0.61	0.79	1.10	0.83	1.04	0.042	1.89
B2FIH6	0.01	0.02	0.01	0.03	0.02	0.02	0.042	1.82
B2FII9	0.01	0.01	0.01	0.01	0.01	0.02	0.004	2.25
B2FIU9	2.67	8.42	7.66	11.23	9.33	10.82	0.045	1.67
B2FJ17	0.05	0.10	0.08	0.13	0.12	0.11	0.025	1.58
B2FJ30	0.13	0.31	0.32	0.03	0.04	0.10	0.022	0.22
B2FJ52	0.01	0.03	0.03	0.04	0.04	0.04	0.037	1.60
B2FJ58	0.02	0.02	0.02	0.01	0.02	0.01	0.038	0.71
B2FJ99	0.00	0.01	0.01	0.03	0.03	0.02	0.021	2.44
B2FJA5	0.02	0.03	0.03	0.04	0.03	0.04	0.047	1.29
B2FJD5	0.03	0.04	0.02	0.05	0.05	0.03	0.045	1.60
B2FJE8	0.11	0.16	0.13	0.20	0.21	0.17	0.011	1.48
B2FJP9	0.04	0.06	0.07	0.09	0.10	0.08	0.013	1.56
B2FJQ8	0.16	0.14	0.14	0.12	0.12	0.10	0.007	0.75
B2FJR0	0.20	0.14	0.16	0.12	0.13	0.09	0.039	0.70
B2FJY2	0.01	0.01	0.01	0.02	0.02	0.02	0.001	2.11
B2FJY7	0.09	0.07	0.09	0.05	0.05	0.05	0.002	0.62
B2FK85	0.02	0.07	0.07	0.10	0.11	0.08	0.035	1.81

B2FK88	0.16	0.30	0.22	0.45	0.38	0.37	0.011	1.77
B2FK94	0.00	0.02	0.02	0.04	0.03	0.02	0.039	2.19
B2FKE4	0.03	0.08	0.06	0.10	0.11	0.08	0.032	1.72
B2FKE8	0.01	0.01	0.01	0.04	0.02	0.03	0.011	3.27
B2FKI7	0.02	0.05	0.04	0.07	0.06	0.06	0.021	1.60
B2FKK2	0.10	0.16	0.17	0.21	0.20	0.20	0.029	1.42
B2FKK6	0.01	0.02	0.03	0.03	0.06	0.04	0.037	2.26
B2FKL5	0.01	0.01	0.01	0.02	0.02		0.037	1.63
B2FKL8	0.01	0.06	0.04	0.09	0.11	0.05	0.046	2.20
B2FKM0	0.01	0.05	0.06	0.09	0.07	0.07	0.037	1.97
B2FKN8	0.02	0.04	0.04	0.09	0.07	0.07	0.005	2.34
B2FKN9	0.03	0.05	0.05	0.10	0.09	0.08	0.003	1.98
B2FKU8	0.02	0.04	0.04	0.07	0.07	0.06	0.008	1.87
B2FKV6	0.01	0.01	0.02	0.03	0.04	0.03	0.003	2.48
B2FL08	0.13	0.12	0.13	0.05	0.05	0.04	0.000	0.36
B2FL10	0.03	0.04	0.05	0.01	0.02	0.01	0.014	0.37
B2FL60	0.02	0.02	0.02	0.05	0.03	0.03	0.041	1.78
B2FL71	0.02	0.06	0.04	0.08	0.07	0.07	0.017	1.83
B2FL74	0.01	0.02	0.01	0.03	0.04	0.03	0.015	2.24
B2FL78	0.02	0.05	0.04	0.05	0.06	0.05	0.045	1.52
B2FL97	0.01	0.03	0.03	0.04	0.04	0.03	0.048	1.66
B2FLB0	0.03	0.04	0.04	0.07	0.06	0.05	0.012	1.62
B2FLB9	0.01		0.01	0.01		0.01	0.015	1.63
B2FLC8	0.07	0.11	0.11	0.18	0.16	0.15	0.010	1.67
B2FLD8	0.01	0.01	0.01	0.01	0.02		0.040	1.36
B2FLE4	0.01	0.02	0.02	0.05	0.05	0.04	0.007	2.70
B2FLE9	0.07	0.07	0.06	0.09	0.11	0.10	0.010	1.52
B2FLG0	0.04	0.07	0.07	0.12	0.10	0.08	0.027	1.68
B2FLG2	0.39	0.33	0.22	0.19	0.17	0.13	0.021	0.52
B2FLQ1	0.02	0.02	0.03	0.01	0.02	0.01	0.038	0.58
B2FLR1	0.22	0.24	0.19	0.31	0.31	0.24	0.032	1.30
B2FLR7	0.01		0.01		0.01	0.01	0.022	0.86
B2FLT7	0.17	0.19	0.18	0.10	0.08	0.09	0.000	0.51
B2FLT8	0.03	0.04	0.04	0.05	0.07	0.07	0.005	1.84
B2FLU6	0.08	0.16	0.09	0.22	0.19	0.15	0.037	1.71
B2FLU7	0.04	0.10	0.05	0.13	0.12	0.09	0.048	1.72
B2FLW7	0.01	0.02	0.03	0.03	0.04	0.03	0.040	1.79
B2FM87	0.02	0.05	0.04	0.06	0.07	0.05	0.029	1.79
B2FMB0	0.01	0.03	0.03	0.05	0.05	0.04	0.020	2.00
B2FMD6	0.02		0.02	0.01	0.01		0.041	0.51
B2FME5	0.02	0.03	0.02	0.03	0.03	0.03	0.014	1.53
B2FME6	0.02	0.02	0.01	0.02	0.02		0.019	1.33
B2FME8	0.03	0.06	0.05	0.16	0.12	0.12	0.002	2.84
B2FMF0	0.03	0.07	0.05	0.10	0.08	0.08	0.020	1.73
B2FMF5	0.01	0.02	0.01	0.03	0.02	0.02	0.044	1.64
B2FMH2	0.02	0.03	0.03	0.04	0.04	0.04	0.024	1.40
B2FMK4	0.01	0.04	0.03	0.05	0.05	0.04	0.032	1.68
B2FMP6	0.05	0.08	0.12	0.14	0.14	0.12	0.035	1.58
B2FMP7	0.05	0.06	0.09	0.12	0.13	0.11	0.005	1.85
B2FMP8	0.03	0.09	0.09	0.15	0.15	0.13	0.012	2.15
B2FMP9	0.03	0.08	0.08	0.14	0.15	0.10	0.033	1.87
B2FMQ2	0.00	0.02	0.02	0.03	0.02	0.03	0.023	2.09
B2FMR4	0.10	0.22	0.20	0.26	0.33	0.30	0.021	1.69
B2FMR5	0.09	0.13	0.10	0.18	0.15	0.17	0.013	1.51
B2FMS4	0.22	0.40	0.28	0.43	0.52	0.45	0.025	1.57
B2FMT2	0.03	0.04	0.03	0.06	0.04	0.05	0.043	1.41

B2FMY5	1.04	1.00	1.05	1.61	1.46	1.21	0.014	1.39
B2FMY6	0.06	0.07	0.12	0.12	0.13	0.13	0.040	1.51
B2FMZ8	0.03	0.07	0.05	0.11	0.08	0.08	0.019	1.92
B2FN25	0.02	0.08	0.07	0.12	0.11	0.09	0.041	1.83
B2FN41	0.01	0.01	0.01	0.01	0.01	0.01	0.047	1.27
B2FN47	0.05	0.04	0.02	0.02	0.02	0.01	0.027	0.36
B2FN55	0.04	0.06	0.03	0.08	0.07	0.06	0.018	1.63
B2FN91	0.06	0.13	0.15	0.21	0.18	0.21	0.018	1.76
B2FN95	0.08	0.03	0.04	0.01	0.01	0.02	0.033	0.27
B2FNA0	0.00	0.01		0.02	0.02	0.02	0.022	2.22
B2FNF2	0.02	0.06	0.06	0.01	0.01	0.01	0.028	0.23
B2FNF7	0.01	0.04	0.05	0.06	0.07	0.05	0.044	1.90
B2FNG6	0.06	0.09	0.06	0.14	0.11	0.14	0.004	1.85
B2FNJ1	0.04	0.12	0.12	0.18	0.24	0.15	0.032	2.01
B2FNJ3	0.01	0.03	0.03	0.05	0.05	0.04	0.014	2.03
B2FNK2	0.07	0.21	0.15	0.28	0.25	0.38	0.025	2.11
B2FNN9	0.01	0.02	0.02	0.04	0.03	0.04	0.014	2.37
B2FNS0	0.09	0.10	0.14	0.13	0.16	0.15	0.032	1.37
B2FNS1	0.06	0.09	0.08	0.15	0.13	0.13	0.003	1.85
B2FNX3	0.09	0.16	0.18	0.26	0.25	0.24	0.008	1.77
B2FNY1	0.01	0.06	0.09	0.13	0.11	0.13	0.014	2.37
B2FNY7	0.03	0.07	0.04	0.08	0.09	0.08	0.016	1.76
B2FNZ1	0.02	0.02	0.02	0.04	0.05	0.03	0.014	1.90
B2FNZ9	0.01	0.02	0.03	0.09	0.06	0.08	0.003	3.47
B2FP02	0.02	0.08	0.07	0.11	0.11	0.09	0.035	1.83
B2FP17	0.50	0.37	0.27	0.22	0.26	0.16	0.044	0.57
B2FP47	0.08	0.11	0.10	0.14	0.16	0.12	0.014	1.47
B2FP48	0.04	0.09	0.08	0.11	0.12	0.13	0.016	1.80
B2FP68	0.06	0.22	0.20	0.26	0.27	0.26	0.049	1.69
B2FP69	0.01	0.01	0.01	0.03	0.02	0.02	0.006	2.12
B2FP70	0.01	0.01	0.06	0.08	0.07	0.07	0.021	2.76
B2FP71	0.04	0.12	0.11	0.14	0.15	0.19	0.034	1.84
B2FP88	0.02	0.05	0.03	0.07	0.09	0.05	0.026	2.06
B2FP98	0.23	0.21	0.31	0.02	0.02		0.005	0.07
B2FPC4	0.04	0.05	0.03	0.03	0.02	0.02	0.021	0.56
B2FPD8	0.03	0.14	0.13	0.18	0.17	0.17	0.049	1.77
B2FPE8	0.02	0.03	0.04	0.05	0.06	0.07	0.005	1.88
B2FPH9	0.07	0.11	0.09	0.16	0.14	0.14	0.007	1.68
B2FPJ1	0.05	0.07	0.07	0.13	0.12	0.12	0.000	1.94
B2FPL6	0.02	0.04	0.04	0.06	0.07	0.06	0.011	1.73
B2FPN5	0.03	0.03	0.02	0.02	0.02	0.01	0.013	0.52
B2FPQ0	0.01	0.01	0.01	0.03	0.03	0.02	0.008	2.35
B2FPQ1	0.01	0.01	0.01	0.02	0.02	0.02	0.003	2.39
B2FPR9	0.05	0.10	0.12	0.15	0.16	0.13	0.035	1.65
B2FPV8	0.04	0.03	0.05	0.05	0.07	0.05	0.032	1.39
B2FPW8	0.06	0.18	0.13	0.26	0.27	0.18	0.027	1.95
B2FPY6	0.01	0.04	0.02	0.04	0.04	0.04	0.047	1.61
B2FQ05	0.06	0.12	0.11	0.15	0.16	0.14	0.027	1.55
B2FQ14	0.00	0.01	0.01	0.01	0.01		0.026	1.80
B2FQ19	0.01	0.04	0.04	0.06	0.07	0.06	0.008	2.11
B2FQ20	0.56	1.40	1.28	1.95	2.01	1.48	0.039	1.68
B2FQ36	0.15	0.19	0.25	0.31	0.33	0.30	0.008	1.60
B2FQ58	0.02	0.05	0.06	0.14	0.09	0.11	0.010	2.71
B2FQ70	0.01	0.02	0.02	0.03	0.04	0.03	0.027	1.84
B2FQ71	0.03	0.04	0.05	0.06	0.05	0.05	0.029	1.45
B2FQ72	0.08	0.10	0.10	0.17	0.15	0.16	0.002	1.67

B2FQ90	0.02	0.03	0.03	0.04	0.03	0.05	0.047	1.64
B2FQH3	0.01	0.04	0.02	0.05	0.04	0.04	0.048	1.71
B2FQH6	0.01	0.02	0.02	0.03	0.06	0.03	0.028	2.73
B2FQH8	0.01	0.05	0.04	0.06	0.06	0.06	0.034	1.83
B2FQL7	0.58	0.57	0.45	0.69	0.69	0.70	0.007	1.31
B2FQM3	0.02	0.04	0.04	0.08	0.10	0.07	0.006	2.47
B2FQN4	0.03	0.12	0.09	0.16	0.13	0.14	0.040	1.81
B2FQR1	0.10	0.19	0.21	0.25	0.26	0.25	0.033	1.53
B2FQU5	0.04	0.09	0.10	0.22	0.22	0.17	0.004	2.66
B2FQU6	0.03	0.07	0.10	0.21	0.22	0.19	0.002	3.06
B2FQU7	0.04	0.07	0.09	0.17	0.19	0.14	0.005	2.49
B2FQX4	0.02	0.02	0.03	0.08	0.05	0.05	0.007	3.07
B2FQY3	0.04	0.16	0.15	0.26	0.29	0.19	0.027	2.08
B2FQY5	0.06	0.07	0.06	0.10	0.11	0.08	0.021	1.52
B2FQZ2	0.01	0.02	0.02	0.03	0.04	0.02	0.025	1.94
B2FR15	0.01	0.01	0.01	0.01	0.01	0.01	0.016	1.15
B2FR21	0.07	0.11	0.09	0.15	0.15	0.13	0.005	1.64
B2FR50	0.09	0.22	0.24	0.38	0.34	0.31	0.017	1.85
B2FR55	0.04	0.07	0.08	0.09	0.10	0.09	0.040	1.46
B2FR74	0.01	0.01	0.01	0.02	0.02		0.016	1.41
B2FR92	0.01	0.01	0.02	0.02	0.02	0.02	0.038	1.38
B2FRF2	0.02	0.07	0.07	0.11	0.13	0.09	0.019	2.02
B2FRK9	0.01		0.01	0.01	0.02	0.01	0.018	1.33
B2FRM5	0.01	0.02	0.02	0.02	0.03	0.02	0.026	1.42
B2FRN8	0.01	0.03	0.03	0.08	0.05	0.05	0.025	2.31
B2FRP1	0.07	0.20	0.13	0.27	0.22	0.23	0.032	1.79
B2FRQ4	0.08	0.13	0.15	0.17	0.20	0.17	0.031	1.50
B2FRS1	0.01	0.02	0.02	0.03	0.03	0.03	0.011	2.22
B2FRS3	0.35	0.32	0.47	0.57	0.56	0.67	0.010	1.58
B2FRS8	0.55	0.34	0.60	0.18	0.23	0.32	0.025	0.50
B2FRT5	0.03	0.03	0.05	0.05	0.07	0.08	0.024	1.85
B2FRV3	0.01	0.06	0.04	0.08	0.07	0.06	0.046	1.90
B2FRW3	0.11	0.07	0.10	0.16	0.18	0.18	0.002	1.92
B2FRX1	0.06	0.10	0.08	0.12	0.11	0.10	0.024	1.43
B2FRZ2	0.02	0.10	0.09	0.19	0.16	0.14	0.015	2.33
B2FRZ3	0.02	0.03	0.02	0.07	0.06	0.04	0.021	2.33
B2FS02	0.01	0.02	0.02	0.03	0.03	0.02	0.012	1.64
B2FS05	0.02	0.02	0.02	0.03	0.03	0.04	0.009	1.75
B2FSE9	0.08	0.09	0.12	0.06	0.06	0.04	0.020	0.55
B2FSF3	0.04	0.12	0.14	0.15	0.18	0.18	0.045	1.67
B2FSF9	0.01	0.01	0.02	0.03	0.03	0.02	0.027	1.92
B2FSG5	0.26	0.31	0.22	0.42	0.36	0.31	0.037	1.37
B2FST5	0.00	0.01	0.00	0.01	0.01	0.01	0.046	1.90
B2FT17	0.02	0.07	0.07	0.11	0.09	0.09	0.041	1.83
B2FT38	0.04	0.08	0.07	0.11	0.09	0.08	0.039	1.53
B2FT49	0.01	0.03	0.02	0.05	0.04	0.03	0.026	1.85
B2FTA3	0.19	0.17	0.12	0.23	0.24	0.19	0.040	1.37
B2FTA7	0.05	0.08	0.09	0.14	0.13	0.10	0.022	1.71
B2FTD1	0.32	0.32		0.22	0.24	0.20	0.004	0.70
B2FTD2	0.99	0.53	0.54	0.15	0.19	0.22	0.016	0.28
B2FTJ0	0.10	0.10	0.07	0.14	0.13	0.10	0.042	1.39
B2FTM1	0.06	0.15	0.20	0.43	0.39	0.34	0.004	2.83
B2FTR8	0.01	0.01	0.02	0.04	0.03	0.03	0.001	2.76
B2FTT5	0.21	0.17	0.12	0.27	0.25	0.20	0.046	1.43
B2FTU5	0.03	0.04	0.05	0.07	0.10	0.06	0.032	1.78
B2FTV4	0.06	0.16	0.16	0.24	0.24	0.20	0.022	1.79

B2FTX1	0.02	0.06	0.06	0.11	0.08	0.08	0.025	1.85
B2FUA1	0.08	0.06	0.08	0.06	0.07	0.04	0.043	0.75
B2FUC3	0.02	0.02	0.02	0.04	0.03	0.03	0.001	1.79
B2FUE8	0.04	0.09	0.06	0.11	0.11	0.09	0.027	1.76
B2FUR4	0.04		0.05	0.02	0.02	0.02	0.011	0.44
B2FUS0	0.01	0.01	0.01	0.02	0.02	0.03	0.011	1.93
B2FUU7	0.05	0.05	0.03	0.07	0.08	0.05	0.046	1.47
B2FUV1	0.10	0.15	0.10	0.05	0.09	0.06	0.049	0.59
B2FUV9	0.02		0.01	0.02	0.02	0.03	0.009	1.74

17

18